THE ROLE OF THE IRE1α PATHWAY IN VASCULAR STIFFENING AND FIBROSIS

By

Victor Tat, B.H.Sc.

A Thesis Submitted to the School of Graduate Studies in Partial Fulfilment of the Requirements for the Degree Master of Science

MASTERS OF SCIENCE (2017) McMaster University, Hamilton, Ontario
(Medical Sciences: Physiology and Pharmacology)

TITLE: The Role of the IRE1α Pathway in Vascular Stiffening and Fibrosis

AUTHOR: Victor Tat, B.H.Sc. Honours (McMaster University)

SUPERVISOR: Dr. Jeffrey G. Dickhout

SUPERVISORY COMMITTEE: Dr. Kjetil Ask
Dr. Joan Krepinsky

NUMBER OF PAGES: xi, 83

ABSTRACT

Background: Vascular stiffening develops with both hypertension and aging, and is a strong predictor of end-organ damage. Excessive deposition of collagen by vascular smooth muscle cells (VSMCs) can lead to decreased compliance of vessels such as the aorta. The IRE1α arm of the unfolded protein response is activated in cells with a secretory phenotype due to its role in augmenting protein folding capacity. We hypothesize that by a similar mechanism, VSMCs transitioning to a collagen-secreting phenotype in response to TGF-β1 require the activation of IRE1. Inhibition of this pathway is hypothesized to reduce collagen secretion and hence prevent the development of fibrosis in the aorta.

Methods: Collagen deposition by VSMCs in vitro was measured using immunoblotting and a Picrosirius Red-based colorimetric assay. Western blot and qRT-PCR were used to assess the expression of ER stress markers. Ex vivo culture of aortic rings was also performed to determine the effect of 4μ8c on TGF-β1-induced vascular stiffening. 12-14 week old male spontaneously hypertensive rats were divided into three treatment groups: 1) No treatment, 2) L-NAME (50 mg/L), and 3) L-NAME and the IRE1α inhibitor 4μ8c (2.5 mg/kg/day i.p.). Aortic compliance after 18 days of treatment was measured ex vivo using a wire myograph to construct tension-diameter curves.

Results: Inhibition of IRE1α endonuclease activity by 4μ8c reduced collagen production in VSMCs stimulated with TGF-β1 or Ang II. A decrease in the expression of the collagen-associated chaperones PDI, GRP78 and GRP94 was observed. Aortic rings

treated with TGF-β1 developed vascular stiffening, which was improved by co-treatment with 4μ8c. SHRs treated with L-NAME for 18 days developed aortic stiffening, which was prevented by daily injections of 4μ8c.

Conclusions: Our data suggest that inhibition of the IRE1α pathway can reduce vascular stiffening and fibrosis by disrupting the collagen biosynthesis pathway in VSMCs.

ACKNOWLEDGEMENTS

I would like to first thank my supervisor, Dr. Jeffrey Dickhout, for your support and guidance over the past two years. The opportunity that you provided for me has made me a better researcher and I appreciate your dedication to helping all members of the lab succeed. To my committee members, Dr. Kjetil Ask and Dr. Joan Krepinsky, thank you for your insightful comments and suggestions that helped to shape this thesis.

This project could not have been completed without the help of Vincent Lu, who taught me everything I know about working with animals. Thank you for helping me with all of the surgeries, injections, and navigating through the plethora of paperwork and forms.

I would like to thank all of the people who made the past two years an enjoyable experience. To Zahraa, Rachel, and Vicki, thank you for your mentorship and for the wealth of advice that you gave me over the years. To Safaa, Jasmine, Sonia, Chandak, Salwa, Ashish and the many, many more people in our St. Joe's research family, thank you for all of the great memories. I wish you all success in your future endeavors, and I hope that we keep in touch.

I would like to finally thank my parents, who have supported me since day one. Thank you for all of the love, time, energy and money that you invested into raising me and getting me to where I am now.

TABLE OF CONTENTS

LIST OF ABBREVIATIONS

4-PBA	4-Phenylbutyric acid
α-SMA	Alpha smooth muscle actin
AA2P	Ascorbic acid-2-phosphate
Ang II	Angiotensin II
ATF6	Activating transcription factor 6
CHOP	C/EBP homologous protein
CKD	Chronic kidney disease
DBP	Diastolic blood pressure
ECM	Extracellular matrix
eGFR	Estimated glomerular filtration rate
ER	Endoplasmic reticulum
ERAD	ER-associated degradation
GRP78	Glucose regulated protein, 78 kDa
GRP94	Glucose regulated protein, 94 kDa
HSP47	Heat shock protein, 47 kDa
ISH	Isolated systolic hypertension
IRE1	Inositol-requiring enzyme 1
L-AA	L-ascorbic acid
L-NAME	Nω-Nitro-L-arginine methyl ester hydrochloride
MMP	Matrix metalloproteinase
mRNA	Messenger RNA
miRNA	Micro RNA
PDI	Protein disulfide isomerase
PERK	Protein kinase RNA-like endoplasmic reticulum kinase
PSR	PicroSirius Red
PWV	Pulse wave velocity
RIDD	Regulated IRE1-dependent decay
SBP	Systolic blood pressure
SHR	Spontaneously hypertensive rat

TUDCA	Tauroursodeoxycholic acid
TGF-β	Transforming growth factor beta
UPR	Unfolded protein response
VSMC	Vascular smooth muscle cell
WKY	Wistar-Kyoto
XBP1(u or s)	X-box binding protein 1 (unspliced or spliced)

LIST OF FIGURES AND TABLES

1. INTRODUCTION

1.1 Hypertension

Hypertension is the leading risk factor for premature death in the world (1). It is defined as a persistent elevation of blood pressure above 140/90 mmHg, and it can lead to end organ damage in the heart, kidneys, blood vessels and brain (2). Hypertension increases the risk of coronary events, stroke, heart failure and chronic kidney disease (CKD) (3). Globally, an estimated 41% of people aged 35-70 years have hypertension, and of those, only 46.5% are aware of the diagnosis (4). In Canada, the prevalence of hypertension in persons aged 12 and older is around 18% (5). 95% of hypertension cases are classified as essential hypertension, which has no identifiable cause (3). Hypertension is strongly associated with aging because of the changes in the structure, function and mechanical properties of the vasculature that result. Patients 50 years of age or older with hypertension tend to develop isolated systolic hypertension (ISH), in which systolic blood pressure (SBP) is elevated above 140 mmHg while diastolic blood pressure (DBP) is less than 90 mmHg (6,7). ISH is less responsive to conventional antihypertensive treatments and thus the development of novel therapeutics that address the underlying cause is important (8). A major contributor to isolated systolic hypertension is arterial stiffening.

1.2 Vascular stiffening

The American Heart Association recently concluded that arterial stiffening is a cause rather than a consequence of hypertension (9). The stiffness of the arterial wall,

particularly in central conduit arteries such as the aorta, is a major determinant of systolic blood pressure.

Arterial stiffening largely results from changes in the composition of the vessel wall that occur with aging. The major wall components that contribute to vascular stiffness are the elastin fibers, collagen fibers and vascular smooth muscle cells (VSMCs) (10,11). At low pressures, the tension in the wall is borne by the elastin fibers, while at higher pressures, the tension is transferred to the less distensible collagen fibers. With aging, the elastin fibers become fragmented and degrade over time while collagen content increases (12). Cross-linking of collagen and elastin fibers by advanced glycation end products can also increase the stiffness of the vessel (13). Fibronectin is another component of the extracellular matrix (ECM) that can increase the stability of the collagen fibers and that can interact with integrins expressed on the VSMCs, enhancing cell-matrix interactions (14). VSMCs themselves contribute to the overall stiffness of the blood vessel by contracting and establishing vascular tone. The overall arterial stiffness that is observed in vivo can be defined as the sum of the passive (intrinsic) stiffness generated by the ECM and the active stiffness produced by vascular tone. In this thesis, we focus on changes in the passive stiffness of blood vessels through the remodelling of the ECM.

The compliance of a blood vessel is represented by its stress-strain relationship (11). As a vessel is gradually distended and deformed, the circumferential stress in the vessel wall increases. This relationship is non-linear, however, because of the transfer of the tension from the elastin fibers to the collagen fibers as described earlier. The elastic modulus can

be derived from this stress-strain relationship to provide information about the intrinsic stiffness of the vessel wall components, independent of geometry (15).

1.2.1 Physiological effects of vascular stiffening

Physiologically, vascular stiffening alters the hemodynamics within the arterial system (16,17). The central conduit arteries act as a cushion to dampen the pulsations generated by the heart and to ensure continuous blood flow in the capillaries throughout the cardiac cycle. This is especially important for the coronary arteries which depend on diastolic blood flow. During systole, a fraction of the stroke volume acts to distend the aorta so that this stored energy can allow the aorta to recoil and propel the remaining blood to the peripheral tissues during diastole. Stiffer arteries lose their ability to dampen the pulsatile energy generated by the heart and thus the pulse wave is transmitted to the peripheral vasculature at a much higher velocity during systole, while there is reduced blood flow during diastole. Accordingly, pulse wave velocity (PWV) is used clinically as a gold standard to assess arterial stiffness. Another feature of arterial hemodynamics is the reflected pressure wave that travels back to the aorta (16,17). The tapering and branching in the arterial tree leads to the generation of these reflected waves. In healthy individuals with low PWV, these reflected waves return to the aorta during end-systole and increase aortic pressure during diastole, which is beneficial for maintaining coronary perfusion. However, in individuals with stiffer arteries and higher PWV, these reflected waves

return to the aorta earlier in systole and overlap with the forward wave, increasing SBP while decreasing DBP.

1.2.2 Vascular stiffening and end-organ damage

The heart, kidneys and brain show the most severe damage resulting from increased aortic stiffness. Elevated SBP increases the left ventricular load, eventually leading to left ventricular hypertrophy (18). The increased oxygen demand of the hypertrophied tissue coupled with the decreased coronary perfusion during diastole results in ischemia, predisposing the individual to heart failure (19–21). This may provide a physiological explanation for the strong association between aortic PWV and future cardiovascular events and all-cause mortality (22). Cardiomyocyte hypoxia can also lead to cell death through apoptosis or necrosis, with scar tissue deposited in its place. The overall result is a loss of cardiac function due to cardiomyocyte loss and a stiffer extracellular matrix.

The kidneys and brain consist of large vascular beds with high flow and low resistance. The loss of the aorta's ability to dampen pulsations generated by the heart results in the transmission of these pulsations to the microvasculature. In the brain, this can lead to microvascular ischemia and tissue damage, increasing the risk of cognitive impairment, dementia, and both ischemic and hemorrhagic stroke (23,24). Similarly, increased pulsatility in the kidneys can damage the glomerulus and lead to proteinuria and chronic kidney disease (CKD). Many population-based studies have observed an association between carotid-femoral PWV and incident CKD (25,26). However, there is still

conflicting evidence regarding the association between aortic stiffness and the estimated glomerular filtration rate (eGFR) within the CKD population (27).

1.3 Fibrosis

One of the mechanisms by which blood vessels become stiffer is through the fibrotic remodelling of the extracellular matrix (ECM) in the vessel wall (17,28,29). The ECM of blood vessels comprises of structural proteins such as collagen, elastin, fibronectin and proteoglycans. A change in the relative abundance of these proteins can lead to changes in the compliance of the vessel. Specifically, a loss of elastin and an increase in collagen can lead to vascular fibrosis and stiffening. The remodelling of the ECM in blood vessels is analogous to fibrotic processes that occur in other tissues such as the lungs, heart and kidneys. The end result of fibrosis is a decline in the function of these organs due to the loss of compliance of the tissue (30).

Fibrosis is characterized by an aberrant wound-healing response that leads to the excessive deposition of scar tissue. At the center of the disease are key pathogenic cells that synthesize and secrete large amounts of ECM proteins. In most cases of tissue fibrosis, the myofibroblast takes on this role. It is derived from a number of progenitors, including epithelial cells, endothelial cells, fibroblasts and circulating fibrocytes. When a tissue is injured, the resultant inflammation leads to the activation of these progenitor cells through transforming growth factor-β (TGF-β) signalling, causing them to differentiate into myofibroblasts that express α-smooth muscle actin (α-SMA), the main

component of their contractile apparatus (31). α-SMA integrates into the F-actin stress fibers of the cell, allowing the myofibroblast to gain a migratory phenotype (32). TGF-β signalling also stimulates the expression of ECM components such as Type I collagen (30). During normal tissue repair, myofibroblast activation is controlled and transient, and it dies by apoptosis once the wound is healed (33). Under pathologic conditions, however, the myofibroblasts persist in the tissue long after the initial injury has been repaired and continue to secrete scarring proteins. (34–36).

Vascular fibrosis presents a special case of this process, as the vascular smooth muscle cell (VSMC), rather than the myofibroblast, plays the major role in the remodelling of the ECM. The phenotypic switch of the VSMC from a contractile state to a synthetic state has led some to argue that the synthetic VSMC is functionally identical to a myofibroblast (37). Angiotensin II may play a larger role in vascular fibrosis compared to other tissues due to its ease of access to the vasculature. Ang II has been shown to stimulate collagen synthesis in VMSCs via the upregulation of TGF-β (38,39). TGF-β, acting in an autocrine fashion, causes the VMSCs to respond in a similar manner to fibroblasts, increasing both collagen and global protein synthesis (38,40–45). Ang II can also activate SMAD signalling pathways independently of TGF-β (46). TGF-β can also induce the expression of matrix metalloproteinases (MMPs) that play an important role in the development of fibrosis and vascular stiffening. MMPs degrade ECM proteins, priming the ECM for remodelling processes to take place (47). In particular, MMP2 activity in the aortic wall increases with aging, along with the levels of active TGF-β1

(48). The precise role of MMPs in fibrosis are still unknown, as both stimulatory and inhibitory effects of MMPs on fibrosis have been observed (47).

1.4 Collagen biosynthesis

The production of type I collagen is a complex process that requires several enzymes and chaperones to ensure proper folding and assembly of the procollagen trimer (49). The procollagen trimer consists of two proα1(I) chains and one proα2(I) chain. The initial association between these three chains is facilitated by protein disulfide isomerase (PDI), which promotes interchain disulfide bond formation. Hydroxylation of proline residues by prolyl-4-hydroxylase promotes the winding of the trimer into a triple helix. Prolyl-4-hydroxylase is dependent on the cofactor L-ascorbic acid, and thus collagen biosynthesis is impaired in conditions of ascorbic acid deficiency such as scurvy. L-ascorbic acid has also been shown to stabilize Type I collagen mRNA in VSMCs while diminishing the expression of elastin (52). During this assembly process, the procollagen chains have been shown to interact with endoplasmic reticulum (ER)-resident chaperones such as GRP78/BiP, GRP94, protein disulfide isomerase (PDI) and HSP47, which bind to nascent procollagen chains and promote their assembly into a triple helix (50,51). Protein disulfide isomerase can act as both a molecular chaperone and an enzyme that catalyzes disulfide bond formation between the procollagen chains (51). These chaperones are known to be localized to the ER, and thus we decided to investigate the stress pathways that may be involved in regulating their expression.

1.5 ER Stress and the UPR

Endoplasmic reticulum (ER) stress and the unfolded protein response (UPR) have been implicated in a number of fibroproliferative diseases, including pulmonary fibrosis (34,53–55), cardiac fibrosis (56) and renal fibrosis (57). A recent study has also implicated ER stress in the aortic stiffening of an Ang II model of hypertension (58). However, the precise mechanisms by which ER stress contribute to the pathology is still being unravelled. The ER is the site of protein translation and folding. It has a finite number of chaperones available to fold newly translated proteins. When the rate of protein translation exceeds the rate of protein folding, unfolded proteins begin to accumulate in the ER lumen, resulting in a state known as ER stress (59). GRP78, an ER-resident protein, is able to detect the presence of unfolded proteins. During ER stress, it dissociates from the ER membrane-bound receptor proteins Inositol-requiring enzyme 1 (IRE1), Activating transcription factor 6 (ATF6) and protein kinase RNA-like endoplasmic reticulum kinase (PERK), resulting in the activation of the UPR. The UPR is a conserved pathway designed to restore protein homeostasis to the ER. It accomplishes this through several mechanisms: i) inhibiting global protein synthesis, ii) degrading unfolded proteins present in the ER, iii) upregulating the expression of protein folding chaperones, and iv) expanding the physical size of the ER (60). These are all adaptive mechanisms that aim to resolve the stress in the ER. If they fail to restore protein homeostasis, the UPR can also activate an apoptotic response through the pro-apoptotic transcription factor C/EBP homologous protein (CHOP).

Each of the three pathways of the UPR has both unique and overlapping functions (59,61). Activation of the PERK pathway results in translation attenuation through the phosphorylation of eIF2α. eIF2α phosphorylation also increases the expression of activating transcription factor 4 (ATF4), which upregulates genes such as CHOP which are involved in the pro-apoptotic phase of the UPR. The ATF6 pathway consists of ATF6α and ATF6β, which translocate from the ER to the Golgi apparatus during ER stress, where they undergo cleavage to release a cytosolic fragment which acts as a transcription factor to upregulate genes involved in ERAD and protein folding. Finally, when IRE1α dissociates from GRP78, it dimerizes and trans-autophosphorylates via its kinase domain. The endonuclease domain of IRE1α then cleaves a 26 nucleotide intron from the mRNA of the transcription factor XBP1. This shifts the reading frame and results in the polypeptide spliced XBP1 (XBP1s), which then translocates to the nucleus and upregulates various genes involved in protein folding, ERAD and protein secretion (59). The endonuclease domain of IRE1α can also degrade the mRNAs of ER-translocating proteins through a process known as regulated IRE1-dependent decay (RIDD). Similar to the translation attenuation conferred by the PERK pathway, RIDD reduces the protein folding demand in the ER, promoting cell survival (62). The IRE1α endonuclease can also degrade premature microRNAs, greatly expanding the number of biological pathways and functions that IRE1α can potentially regulate (63). IRE1α can also promote apoptosis through the activation of apoptosis signal-regulating kinase 1 (ASK1) and JUN N-terminal kinase (JNK) (59). Since the diverse activities of IRE1α encompass both pro-survival and pro-apoptotic pathways, some have considered it to be

an important cell fate regulator, mediating the switch from the adaptive to the apoptotic phase of the UPR (62,64). During prolonged ER stress, the RIDD activity of IRE1α begins to degrade the mRNA of the same UPR target genes that had been upregulated by XBP1s and the other UPR activators (62,64). This increases ER stress, marking the switch from the adaptive to the apoptotic phase.

In this thesis, we focus on the role that the IRE1α pathway plays in the development of vascular stiffening and fibrosis. IRE1α activation has been observed in cells with a secretory phenotype, such as pancreatic β-cells (65), macrophages (66) and plasma cells (67,68). By the same logic, we hypothesize that cells involved in the secretion of ECM proteins also require the activation of this pathway. This hypothesis can be tested by inhibiting the function of IRE1α and observing the subsequent effect on collagen biosynthesis. Given the structure of IRE1, inhibitors generally target either the endonuclease domain or the kinase domain of the protein. Currently, several specific small molecule inhibitors of the endonuclease domain have been identified: 4μ8c and STF-083010 are able to inactivate the endonuclease activity of IRE1α by forming a Schiff base with K^{907}, a lysine residue in the RNase active site (69). 4μ8c forms a more stable Schiff base with K^{907} that is less susceptible to hydrolysis compared to STF-083010. Thus, 4μ8c will be used for our subsequent in vivo experiments. Other drugs have been used to inactivate IRE1α through its kinase domain. Sunitib and Sorafinib are FDA-approved broad spectrum kinase inhibitors that interact with the ATP-binding pocket in the kinase domain. Although these compounds lack specificity to IRE1, they have been shown to be effective at blocking XBP1 splicing (70).

1.6 ER stress and fibrosis

ER stress and the UPR have been implicated at the various stages in the pathogenesis of fibrosis, including the initial injury to the tissue, the inflammatory response, and the remodelling phase. The role of ER stress in tissue injury is largely attributed to the ability of prolonged ER stress to initiate apoptosis in cells through the transcription factor CHOP. This has been observed in acute kidney injury (71), post-myocardial infarctions (72), and bleomycin-induced pulmonary fibrosis (73). A diverse range of agents and conditions are capable of inducing ER stress, including toxic compounds, infections, hypoxia, and endogenously produced soluble mediators. In blood vessels, smooth muscle cell apoptosis can be mediated by ER stress and can drive vascular remodelling and fibrosis through the release of pro-fibrotic factors such as IL-6 and TGF-β (58,74). Many studies have used chemical chaperones such as 4-PBA and TUDCA to reduce global ER stress, preventing cellular apoptosis and subsequently inhibiting fibrosis (56,58,75). Our group and others have further shown that oral administration of 4-PBA lowers blood pressure in the spontaneously hypertensive rat (SHR) by improving endothelium-dependent vasodilation in resistance arteries (71,76). A reduction of ER stress markers including CHOP was observed in these vessels. As discussed in the previous section, IRE1α can also play a major role in the regulation of cell fate. While XBP1s mediates the pro-survival response, prolonged ER stress can result in apoptotic signalling from IRE1. Consistent with this, deletion of XBP1 from the liver has been shown to exacerbate liver injury and apoptosis due to the elimination of adaptive signalling from IRE1α (77).

There has also been much interest in the role of ER stress and the UPR in cardiac hypertrophy, which acts as a precursor to cardiac fibrosis. Similar to other tissues, CHOP-deficient mice demonstrated reduced cardiac hypertrophy, cardiomyocyte apoptosis and cardiac fibrosis in response to pressure overload (78). XBP1 has also been implicated in cardiac hypertrophy, although there is conflicting evidence as to whether it plays a contributory or protective role (79–81).

The inflammatory response acts as a mediator between the initial tissue injury and the subsequent fibrotic remodelling. T cell and macrophage infiltration is a hallmark of this response and has been observed in renal and cardiac fibrosis. Inflammation has been linked to the development of hypertension and the associated vascular stiffening (82,83). A recent study demonstrated that M2 macrophages accumulate in the aortic wall during Ang II infusion in mice and actively contribute to the vascular remodelling process through the secretion of TGF-β1, fibronectin and MMPs (83). The IRE1α and PERK pathways of the UPR can activate the transcription factor NF-κB, a major regulator of inflammation (84). Furthermore, we have recently observed that the UPR can modulate the polarization and cell fate of M2 macrophages in a model of bleomycin-induced pulmonary fibrosis (55). These results highlight the ability of the UPR to regulate the inflammatory response and ultimately the differentiation and activity of the myofibroblasts and smooth muscle cells that contribute to the fibrotic remodelling.

The present study focuses on the final stage of the development of fibrosis, in which cells such as myofibroblasts and smooth muscle cells become activated to synthesize and secrete copious amounts of ECM proteins. The increase in protein translation in these

cells necessitates that the cells respond by increasing their protein folding capacity in order to restore homeostasis to the ER. ER stress induction alone has been shown to be sufficient to induce myofibroblast differentiation (85) or epithelial-to-mesenchymal transition (36,86,87). Cells undergoing myofibroblast differentiation through TGF-β1 stimulation exhibit an elevation of ER stress and UPR markers such as GRP78, CHOP and XBP1 splicing (34,88). Heindryckx et al. recently demonstrated that the IRE1α arm of the UPR regulates TGF-β1-induced myofibroblast differentiation by increasing the size of ER and by indirectly increasing the expression of αSMA through microRNA regulation (88). They showed that inhibition of IRE1α using the small molecule inhibitor 4μ8c was able to prevent fibrosis in a model of CCl_4-induced liver cirrhosis and a model of TGF-β-induced skin fibrosis. A recent study also found that overexpression of spliced XBP1 in hepatic stellate cells was sufficient to induce Type I collagen synthesis (89). We propose here that the IRE1α pathway can also regulate collagen synthesis by regulating the expression of the various chaperones involved in the maturation and folding of collagen. Many of these chaperones, including GRP78, GRP94, PDI and calreticulin are direct target genes of the transcription factor XBP1s (65,90). Indeed, several of these chaperones have already been shown to be necessary for collagen biosynthesis; cells deficient in calreticulin are unable to produce and secrete collagen, with the unfolded collagen molecules accumulating in the ER (91). Since calreticulin and the other collagen-folding chaperones are downstream of IRE1, we hypothesize that inhibition of IRE1α will have a similar effect in preventing the maturation and secretion of collagen.

1.7 Hypothesis

We hypothesize that activation of the IRE1α pathway is required for the production and secretion of collagen from VSMCs, leading to vascular fibrosis and stiffening (**Figure 1**). This hypothesis will be tested using three model systems of vascular stiffening: 1) an in vitro culture of rat aortic smooth muscle cells, 2) an ex vivo organ culture of rat aortas, and 3) an in vivo model of malignant hypertension and vascular stiffening. In these models, the IRE1α pathway will be inhibited using small molecule inhibitors of the IRE1α endonuclease. Specific objectives for each model are as follows:

1) In vitro model: Using ascorbic acid, TGF-β1 and Ang II to induce collagen synthesis in rat VSMCs, the effect of the IRE1α inhibitors 4μ8c and STF-083010 on collagen synthesis will be measured using a dot blot for Type I collagen and a picrosirius red-based colorometric assay. The effect the IRE1α inhibitors on key chaperones in the collagen biosynthesis pathway will be assessed.
2) Ex vivo model: Aortic rings isolated from a young WKY rat will be cultured in the presence of TGF-β1 to induce collagen production and fibrosis of the vessel. Compliance of the cultured rings will be assessed using a wire myograph. The effect of co-treatment with IRE1α inhibitors will be studied.
3) In vivo model: Spontaneously hypertensive rats will be administered with L-NAME to induce severe hypertension. Rats will be given daily injections of the IRE1α inhibitor 4μ8c, and compliance of the aorta and carotid artery will be measured at sacrifice using a wire myograph. Fibrosis in the aorta, heart and kidneys will be assessed.

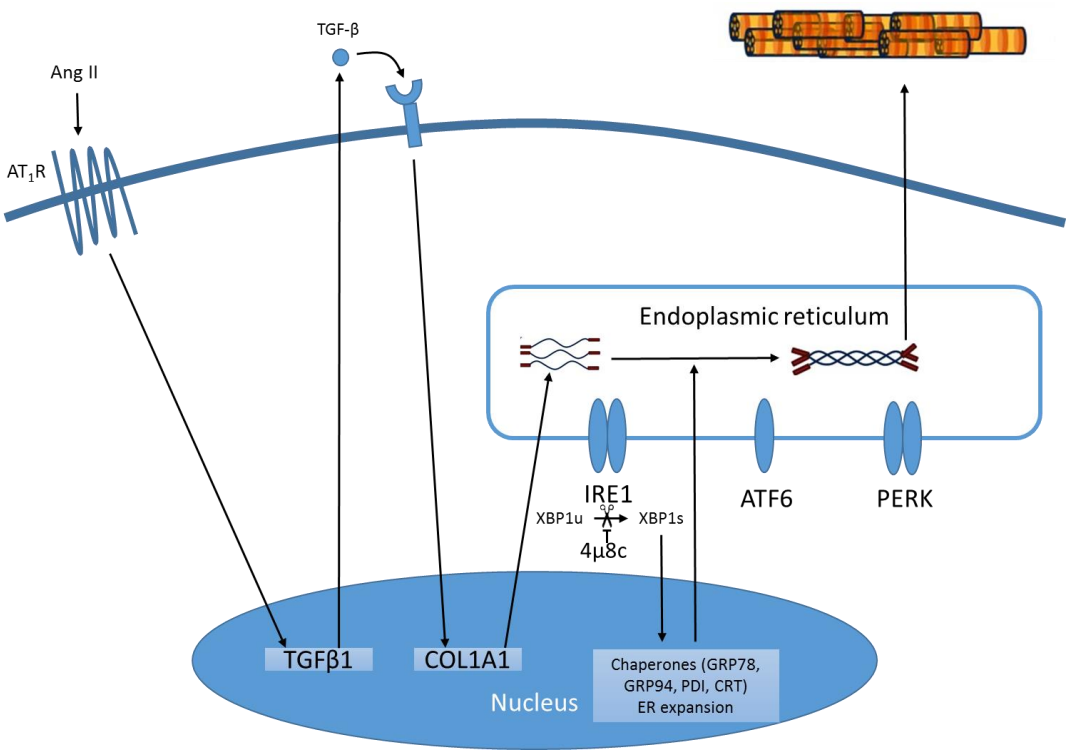

Figure 1. Proposed model for the role of IRE1 in collagen biosynthesis. Angiotensin II, acting through the AT_1 receptor, can upregulate the expression of TGF-β1 in VSMCs. TGF-β1 is secreted in an inactive form as part of a latent complex. Through a number of possible mechanisms, TGF-β1 can be released from this complex and can then act in an autocrine fashion to stimulate the TβRI receptor. Signaling through the Smad pathway, the expression of collagens such as Type I collagen can be induced. The subsequent increase in protein translation can result in an accumulation of unfolded proteins due to the saturation of the available protein folding chaperones. In this state of ER stress, the UPR is activated through the IRE1, ATF6 and PERK pathways. We propose here that the IRE1 pathway, and its downstream transcription factor XBP1s, can increase the expression of chaperones required for collagen synthesis such as GRP78, GRP94, PDI and calreticulin. Hence, inhibition of the IRE1 endonuclease domain with the small molecule inhibitor 4μ8c can prevent the splicing of XBP1 mRNA, reducing the induction of the collagen folding chaperones and ultimately preventing collagen secretion from the cell.

2.0 MATERIALS AND METHODS

2.1 Smooth muscle cell isolation and culture

VSMCs were isolated from the aortas of 5 week old WKY rats using the explant method (92). The thoracic aorta was removed from the animal and placed in ice-cold 5x Antibiotics-Antimycotics solution (ThermoFisher). The adventitia was gently removed and the aorta was cut longitudinally. The endothelial layer was removed by gentle scraping with forceps. The aorta was cut into 3 mm^2 squares and placed on a 6 well plate in DMEM/F12 medium containing 10% FBS. Explants were incubated undisturbed in a 5% CO_2 incubator at 37^oC for 1 week and then passaged. Cells between passages 5 and 10 were used for experiments.

2.2 Animals

12-14 week old male SHRs were used to determine the effect of pharmacological IRE1α inhibition on L-NAME-induced vascular stiffening. They were maintained on a 12-hour light-dark cycle with rat chow and water ad libitium. Animals were implanted with radio-telemetry devices (Data Science International, Netherlands) one week before the start of the study. Animals were randomized into one of three groups (n = 6 per group): 1) No treatment, 2) L-NAME (50 mg/L in drinking water, Sigma-Aldrich), or 3) L-NAME + 4μ8c (2.5 mg/kg/day i.p., Millipore). 4μ8c was administered in a vehicle of 10% DMSO, 10% Tween-80 and 80% normal saline. Animals in Group 2 received daily injections of the vehicle. All animals were fed a normal chow diet. At 18 days, animals were sacrificed, organs were harvested and the aorta was collected for mechanical and

structural analysis. All animal work was performed according to the McMaster University Animal Research Ethics Board guidelines.

2.3 XBP1 splicing assay

Total RNA was extracted from cultured cells and rat tissues using the TRIzol reagent (ThermoFisher) according to manufacturer's instructions. RNA concentration and purity were measured using a Nanodrop ND-1000 spectrophotometer (NanoDrop Technologies, Inc.). RNA was reverse transcribed using the High-Capacity cDNA Reverse Transcription Kit (Applied Biosystems) according to manufacturer's instructions. For qualitative assessment of XBP1 splicing, cDNA was amplified using recombinant Taq polymerase (Invitrogen) and primers for total XBP1: Forward 5'-AAACAGAGTAGCAGCGCAGACTGC-3', Reverse 5'-GGATCTCTAAAACTAGAGGCTTGGTG-3'. PCR products were digested with PstI for 1 h at 37^{o}C, separated on a 2% agarose gel, and visualized by Safe-Red (ABM, Inc.) and the ChemiDoc XRS+ system (BioRad).

2.4 qRT-PCR analysis

For qRT-PCR, cDNA was amplified using the Fast SYBR Green Master Mix (ThermoFisher) and analyzed with 7500 Software. The primers used were as follows: spliced XBP1 (Forward 5'-CTGAGTCCGAATCAGGTGCAG-3', Reverse 5'-ATCCATGGGAAGATGTTCTGG-3'), GRP78/BiP (Forward 5'-TGGGTACATTTGATCTGACTGGA-3', Reverse 5'-CTCAAAGGTGACTTCAATCTGGG-3'), and 18S (Forward 5'-

GTTGGTTTTCGGAACTGAGGC-3', Reverse 5'-GTCGGCATCGTTTATGGTCG-3'). 18S was used as an internal control for normalization.

2.5 Immunoblotting

Immunoblotting was performed as previously described (36,93). Briefly, cells were lysed in 1x Laemmli buffer and protein content was quantitated using the BioRad DC Protein Assay (BioRad, Mississauga, Canada). Proteins were separated by SDS-PAGE under reducing conditions on a 7.5% gel and transferred to a PVDF membrane using the Trans-Blot Turbo Semi-Dry Transfer system (Bio-Rad, Richmond, CA, USA). Membranes were blocked with 5% milk and incubated with primary antibodies: β actin (A-2228, 1:5000, Sigma-Aldrich, St. Louis, MO, USA), KDEL (SPA-827, 1:1000, Stressgen, Victoria, Canada), HSP47 (H-300, 1:1000, Santa-Cruz, Dallas, TX, USA), PDI (SPA-891, 1:1000, Enzo, Farmingdale, NY, USA), and CHOP (B-3, Santa-Cruz, Dallas, TX, USA). Membranes were then washed in TBST and incubated with a horseradish peroxidase-conjugated secondary antibody (Bio-Rad), followed by development with ECL Western Blotting Detection Reagents (GE Healthcare, Mississauga, Canada). Densitometric analysis was performed with Image-Lab Software (Bio-Rad) and band intensities were normalized against β-actin.

2.6 Collagen dot blot

Collagen synthesis by VSMCs was assessed using a dot blot method adapted from Rodriguez et al (94). Briefly, cells were cultured in the presence of 100 μg/ml L-ascorbic acid for 72 h. The monolayer was then washed once with PBS and cells were scraped

from the plate and resuspended in 0.5 M acetic acid. The sample was briefly sonicated at 23 kHz. 10 µl of each sample was then spotted onto a nitrocellulose membrane. The membrane was dried and then stained with Ponceau S solution for assessment of total protein. The membrane was blocked in 5% milk-0.1% Tween-20 in TBS for 30 min, and incubated with monoclonal anti-Type I Collagen (Sigma-Aldrich, 1:1000) overnight at 4^{o}C. The membrane was then washed, incubated with a horseradish peroxidase-conjugated goat anti-mouse IgG antibody (Bio-Rad, 1:10000), and developed with ECL Western Blotting Detection Reagents (GE Healthcare, Mississauga, ON). Densitometric analysis was performed with Image-Lab Software (Bio-Rad).

2.7 Sirius Red spectrophotometric assay

Collagen synthesis was also measured using a Picro-Sirius Red-based assay as previously described (95). Briefly, cells cultured on a 96 well plate were fixed in methanol for 10 minutes at -20^{o}C. Cells were washed once with PBS and incubated with DAPI (1 µg/ml) for 10 minutes to stain the nucleus and normalize for cell number. Fluorescence at 358/461 nm was measured using a Gemini XPS Microplate Reader (Molecular Devices). Cells were then incubated with Picrosirius Red stain (0.1% Direct Red 80 in saturated picric acid) for 1 h at room temperature. After the staining solution was removed, the cells were washed three times with 0.1% acetic acid and then imaged. The dye was then eluted with 0.1 N NaOH for 10 minutes on a rocking platform. Absorbance at 540 nm was measured using a Spectramax Plus Microplate Reader (Molecular Devices).

2.8 Determination of collagen content in aortic tissues

The wet weight of aortic tissues was determined. Tissues were then placed in 100 µl of a 0.5 M acetic acid solution and incubated at 65ºC for 5 hours to promote disintegration of the tissue. 20 µl of the resultant solution was loaded onto a 96 well plate along with collagen standards ranging from 12.5 µg to 200 µg. The plate was dried overnight at 55ºC and subsequently incubated with Picrosirius Red as previously described.

2.9 Aortic ring assay

Aortic ring culture methods were adapted from Nicosia (96) and Lomashvili (97), in which aortic rings were used to study angiogenesis and vascular calcification, respectively. Thoracic aortas were removed in a sterile manner from 5-7 week old WKY rats. The adventitia was removed by dissection and the aorta was cut into 2-3 mm rings and placed in serum-free LG DMEM/F12 containing 2.5X Antibiotic-Antimycotics (ThermoFisher). Aortic rings were incubated for 5 days in the presence of TGF-β1 (5 ng/ml) and 4µ8c (30 µM), with a media change after 2 days. Compliance was then measured using a wire myograph.

2.10 Measurement of vascular stiffness

Vessels were mounted on a steel wire myograph and incubated in Ca^{2+}-free Hank's Basic Salt Solution containing 100 µM sodium nitroprusside to ensure maximum relaxation. Vessels were then stretched incrementally to predefined tensions from 0.1 to 8 g. Images of the vessels at each incremental tension were captured and lumen diameters were measured with ImageJ software. Circumferential stress (σ) was calculated as F/tl, where

F is the tension in the vessel wall, *t* is the radial thickness of the vessel wall and *l* is the axial length of the aortic ring. Circumferential strain (ε) was calculated as $(D - D_0)/D_0$ where D is the lumen diameter at a given tension and D_0 is the initial diameter under maximally relaxed conditions. The stress-strain data was fitted to an exponential equation $\sigma = \sigma_0 e^{k\varepsilon}$, where σ_0 is the initial stress in the relaxed vessel and k is a constant. Incremental elastic modulus was calculated from the first derivative of the stress-strain equation: $E = \frac{d\sigma}{d\epsilon} = k\sigma_0 e^{k\epsilon}$.

2.11 Histology

Tissues were fixed in 4% paraformaldehyde and subsequently embedded in paraffin. 4 μm sections were cut, deparaffinized, and stained with Picro-Sirius Red for 1 hour, followed by two washes with 0.5% acetic acid. Slides were imaged using a light microscope and structural analyses were performed using ImageJ. Collagen area density was calculated by dividing the PSR-stained area by the total area of the vessel.

2.12 Statistical analysis

Values are expressed as mean ± SEM. Statistical analyses were conducted using GraphPad Prism 6. For comparisons between the means of two groups, a Student's *t*-test was used. For comparisons of more than two groups, a one-way ANOVA was used, followed by a Newman-Keuls post hoc analysis for multiple comparisons. For analysis of data with two independent variables (treatment group and time), a two-way ANOVA was used.

3. RESULTS

3.1 IRE1α endonuclease activity is required for collagen synthesis in VSMCs.

3.1.1 Assessment of the ability of 4μ8c to block XBP1 splicing in VSMCs

Aortic VSMCs were isolated from normotensive WKY rats and used for in vitro experiments. To determine the role of the IRE1α pathway in the synthesis of collagen by VSMCs, the IRE1α endonuclease inhibitors 4μ8c and STF-083010 were used. To test the ability of 4μ8c to block XBP1 splicing, VSMCs were treated with the ER stress inducer tunicamycin for 6 h with or without pre-treatment by 4μ8c or STF-083010. XBP1 splicing was assessed by RT-PCR followed by digestion with PstI and electrophoretic separation on a 2% agarose gel. The PstI restriction site is only present in the unspliced variant of XBP1, and thus digestion with PstI results in a 310 bp band (98). 4μ8c and STF-083010 were observed to reduce the ratio of spliced-to-unspliced XBP1 in cells treated with tunicamycin (**Figure 2A)** or TGF-β1 (**Figure 2B**). As measured by qRT-PCR, tunicamycin induced the expression of spliced XBP1 at 6 h, which was blocked by pre-treatment with 4μ8c (**Figure 2C**). Similarly, 4μ8c reduced the expression of spliced XBP1 after a 24 h treatment with TGF-β1 or Angiotensin II (**Figure 2D**).

3.1.2 Effect of IRE1α inhibition on collagen production by VSMCs

To test the hypothesis that IRE1α activation is necessary for collagen production in VSMCs, cells were stimulated with either L-ascorbic acid, TGF-β1 or Angiotensin II to induce collagen synthesis, and co-treated with either 4μ8c or STF-083010 to inhibit IRE1α endonuclease activity. Collagen production was measured using both a PicroSirius

Red-based colorimetric assay and a dot blot for Type I collagen. In the presence of 10% FBS, L-ascorbic acid (L-AA) and its derivative L-ascorbic acid-2-phosphate (AA2P) were able to induce collagen synthesis and deposition, which was inhibited by 4μ8c (30 μM) and STF-083010 (60 μM) **(Figure 3)**. In conditions of reduced serum, both TGF-β1 and Angiotensin II induced collagen synthesis when co-treated with AA2P, which was again inhibited by co-treatment with 4μ8c or STF-083010 **(Figure 4)**. The PSR-based assay demonstrated linearity up to 200 μg of collagen (**Figure S1A**). DAPI fluorescence also displayed a linear correlation with cell number up to 70000 cells (**Figure S1B**).

3.1.3 Effect of IRE1α inhibition on the expression of collagen-associated chaperones

To elucidate how IRE1α blockade leads to the inhibition of collagen production in VSMCs, the expression of chaperones involved in collagen biosynthesis was measured by western blotting and qRT-PCR. The chaperones GRP78, GRP94 and PDI have been shown to interact with collagen during biosynthesis (50,51). ER stress inducer, tunicamycin was used to induce these chaperones. In cells treated with tunicamycin for 24 h, GRP78, GRP94 and PDI expression were increased. This increase was blunted by co-treatment with either of the IRE1α inhibitors, 4μ8c or STF-083010 (**Figure 5**). Cells induced to increase collagen biosynthesis with either TGF-β1 or Ang II in the presence of AA2P had elevated GRP78 mRNA at 24 h, which was reduced by 4μ8c (**Figure 6**). At the protein level, GRP78, GRP94, and PDI were elevated by TGF-β1 and repressed by co-treatment with 4μ8c, which had also repressed collagen biosynthesis. These findings are consistent with the hypothesis that inhibition of IRE1α reduces collagen biosynthesis by repressing the expression of necessary chaperones for its production.

3.1.4 IRE1α endonuclease activity is required for collagen synthesis in renal fibroblasts

To determine if our findings are translatable to other cell types, we performed similar experiments in renal fibroblasts isolated from Sprague-Dawley rats. In renal fibroblasts, AA2P and TGF-β1 act synergistically to increase collagen synthesis and deposition, which is inhibited by co-treatment with 4μ8c (**Figure 7**).

3.2 Inhibition of IRE1α endonuclease activity prevents the development of TGF-β-induced vascular stiffening of cultured aortic rings

An ex vivo model of vascular stiffening was used to further test our hypothesis. 5 week old WKY rats were sacrificed and aortas were harvested. After dissection of perivascular fat, aortas were sectioned into 2-3 mm rings and placed into DMEM/F12 media containing 1% FBS. Aortic rings were then treated with either TGF-β1 (5 ng/ml) in the presence or absence of 4μ8c (30 μM). Vascular compliance was measured after 5 days of treatment using a wire myograph. A leftward shift in the stress-strain relationship was observed in the vessels treated with TGF-β1, which was rescued by co-treatment with 4μ8c (**Figure 8A**). The plot of incremental elastic modulus versus stress is indicative of the stiffness of wall components (collagen, elastin and VSMCs) independent of the vessel geometry (15). The slope of the elastic modulus-stress line was significantly increased in the TGF-β1 group (2.639±0.047) compared to the Vehicle (2.283±0.064) and the TGF-β1+4μ8c group (2.243±0.051), indicative of increased vascular stiffness (**Figure 8B and 8C**). However, no difference was found when collagen content was measured in the vessels (**Figure 8D and 8E**).

3.3 Inhibition of IRE1α endonuclease activity improves vascular compliance in L-NAME-treated SHRs.

3.3.1 IRE1α inhibition does not affect the L-NAME-induced elevation of blood pressure and heart rate in SHRs.

To test our hypothesis in vivo, the SHR/L-NAME model of vascular stiffening was used. 12-14 week old SHRs were implanted with radiotelemetry devices and treated with the nitric oxide synthase inhibitor L-NAME for 18 days. Rats were given daily injections of either vehicle or 4μ8c (2.5 mg/kg/day i.p.). Blood pressure was significantly increased in the SHR after 6 days of L-NAME treatment compared to baseline (**Figure 9**). At Day 6, SBP had increased from 187.4±5.4 mmHg to 228.0±15.5 mmHg ($p<0.05$) and DBP from 134.8±6.5 mmHg to 174.5±13.6 mmHg. At Day 14, SBP and DBP reached a peak of 262.6±13.9 mmHg and 210.4±14.8 mmHg, respectively. Heart rate was also significantly elevated after 14 days of L-NAME treatment (377.6±21.4 mmHg vs 312.7±3.0 mmHg at baseline, $p<0.05$) and remained elevated until the end of the study (**Figure 9D**). Pulse pressure was not affected by L-NAME treatment (**Figure 9C**). 4μ8c did not have an effect on the L-NAME-induced elevation in blood pressure or heart rate. In the L-NAME+4μ8c group, SBP increased from 166.6±8.4 mmHg at baseline to 216.7±4.8 mmHg at Day 6 while DBP increased from 124.7±5.5 mmHg at baseline to 166.2±8.2 mmHg at Day 6. SBP and DBP peaked at 232.3±5.4 mmHg and 192.1±17.0 mmHg, respectively, at Day 9.

3.3.2 IRE1α inhibition improves vascular compliance in SHRs with malignant hypertension

Aorta and carotid arteries were harvested from the animals at sacrificed and vascular stiffness of maximally relaxed vessels was measured using a wire myograph. Both the aorta and the carotid artery of L-NAME-treated SHRs demonstrated a leftward shift in the stress-strain relationship, indicative of increased vascular stiffness (**Figure 10A and 10D**). The slope of the incremental elastic modulus versus stress line was increased in the aorta of the L-NAME group compared to the NT group (4.696±0.054 vs. 4.090±0.055, $p<0.05$) and decreased in the L-NAME+4μ8c group compared to the L-NAME group (3.970±0.129, $p<0.05$) (**Figure 10B and 10C**). In the carotid artery, there was no difference in the slope of the elastic modulus-stress line between the L-NAME group and the non-treated controls, but the slope of the L-NAME+4μ8c group was significantly lower compared to the other two groups (14.42±0.59 vs. 20.35±0.75 in the L-NAME group, $p<0.05$), indicating reduced stiffness (**Figure 10E and 10F**).

3.3.3 IRE1α inhibition prevents the accumulation of collagen in the aorta of SHRs with malignant hypertension

To assess blood vessel structure, aortas and carotid arteries were stained with Picrosirius Red and imaged using a light microscope (4x magnification) (**Figure 11A and 11C**). Lumen area, medial cross-sectional area and intimal-medial thickness were greater in the L-NAME group compared to the NT group (**Table 1**). Medial cross-sectional area and intimal-medial thickness, but not lumen area, were reduced in the L-NAME+4μ8c group.

To measure collagen content in the aortas of these animals, aortic rings were first weighed for determination of wet weight and then homogenized in a dilute acetic acid solution. Collagen content in the homogenate was measured using the PSR-based colorometric assay. Collagen content was significantly increased in the L-NAME group (67.31±1.09 µg/mg tissue) compared to the NT group (55.25±8.01 µg/mg tissue) and the L-NAME+4µ8c group (47.10±2.88 µg/mg tissue) (**Figure 11B**).

In the carotid arteries, there were no differences in lumen area or medial area among the three groups. A 10% reduction in media-lumen ratio and intimal-medial thickness was observed in the L-NAME+4µ8c group compared to the L-NAME group (**Table 1**). Collagen area density was quantified from the PSR-stained tissues. An increase in collagen density was observed in the L-NAME group, while this was reduced in the L-NAME+4µ8c group (**Figure 11D**). However, the differences were not statistically significant ($p=0.10$).

3.3.4 Assessment of ER stress and UPR activation in aortic tissues

To assess the expression of collagen-associated chaperones in the aorta, aortic tissue lysates were analyzed with qRT-PCR. Spliced XBP1 expression was elevated in the L-NAME group and reduced in the L-NAME+4µ8c group ($p<0.05$) (**Figure 12A**). GRP78 mRNA was observed to be increased in the L-NAME-treated and decreased in the L-NAME+4µ8c group (**Figure 12B)**. However, these differences were not statistically significant.

3.3.5 Assessment of end-organ damage in animal model of vascular stiffening

The SHR/L-NAME model is a model of hypertension-induced end-organ damage. Since vascular stiffness increases the risk of end-organ damage, we hypothesized that 4μ8c would reduce the damage in the heart. Animals in the L-NAME+4μ8c group had reduced cardiac hypertrophy compared to the L-NAME group (4.293±0.438 vs. 4.804±0.222 mg HW/g BW, $p<0.05$) (**Figure 13A**). Animals in the L-NAME group developed severe fibrosis in the left and right ventricles as visualized by PSR staining (**Figure 13B**). Cardiac fibrosis was reduced in the 4μ8c-treated animals ($p<0.05$) (**Figure 13C**).

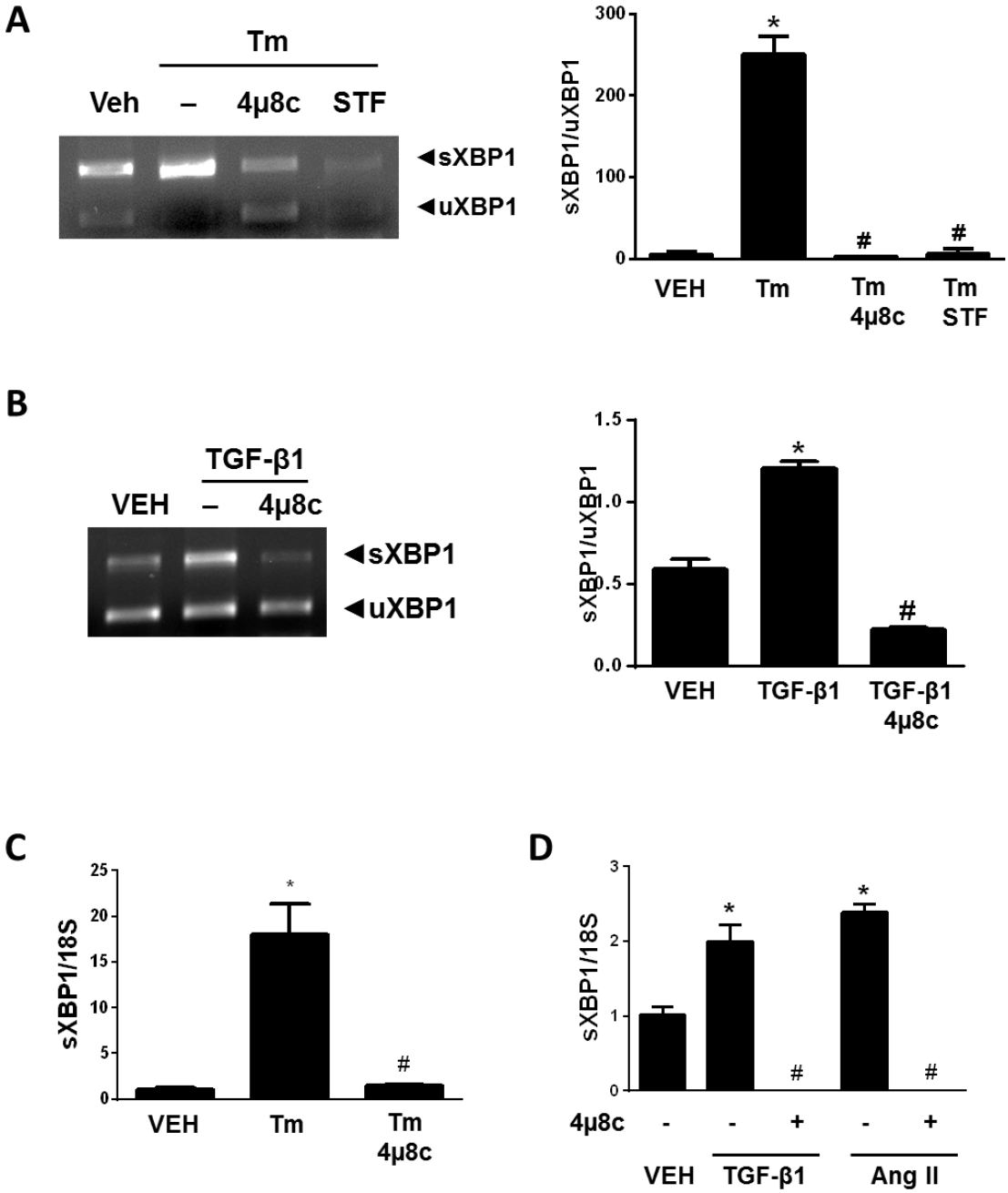
A
Tm
Veh
–
4μ8c
STF
◄sXBP1
◄uXBP1
sXBP1/uXBP1
300
200
100
0
*
#
#
VEH
Tm
Tm 4μ8c
Tm STF
B
TGF-β1
VEH
–
4μ8c
◄sXBP1
◄uXBP1
sXBP1/uXBP1
1.5
1.0
0.5
0.0
*
#
VEH
TGF-β1
TGF-β1 4μ8c
C
sXBP1/18S
25
20
15
10
5
0
*
#
VEH
Tm
Tm 4μ8c
D
sXBP1/18S
3
2
1
0
*
*
#
#
#
4μ8c
-
-
+
-
+
VEH
TGF-β1
Ang II

Figure 2. 4μ8c and STF-083010 block IRE1α-mediated XBP1 splicing. WKY VSMCs were treated with tunicamycin (1 μg/ml) and either 4μ8c (30 μM) or STF-083010 (60 μM) for 6 h. In a second experiment, WKY VSMCs were treated with TGF-β1 (5 ng/ml) or Ang II (1 μM) and 4μ8c (30 μM) for 24 h. (A, B) Agarose gel for assessment of XBP1 splicing and densitometric quantification. (C, D) qRT-PCR analysis of XBP1 splicing in tunicamycin (C) and TGF-β1 and Ang II-induced ER stress (D). Data is presented as mean ± SEM. *, $p<0.05$ vs. Vehicle; #, $p<0.05$ vs. Tm (A) or TGF-β1 (B); †, $p<0.05$ vs. Ang II (B).

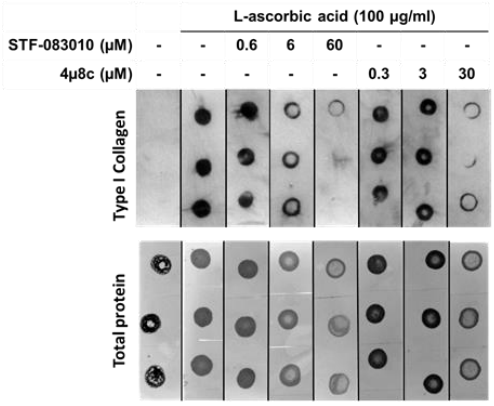

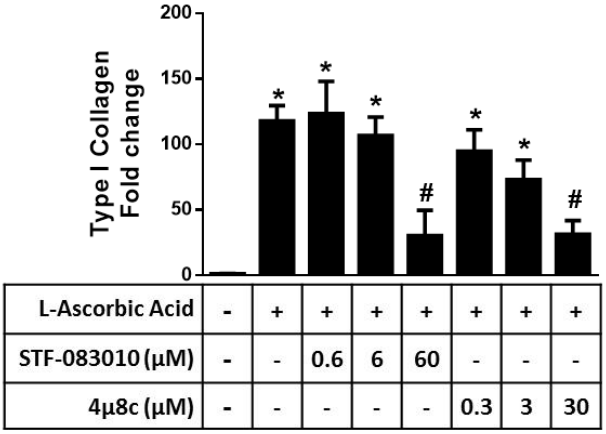

L-Ascorbic Acid	-	+	+	+	+	+	+	+
STF-083010 (µM)	-	-	0.6	6	60	-	-	-
4µ8c (µM)	-	-	-	-	-	0.3	3	30

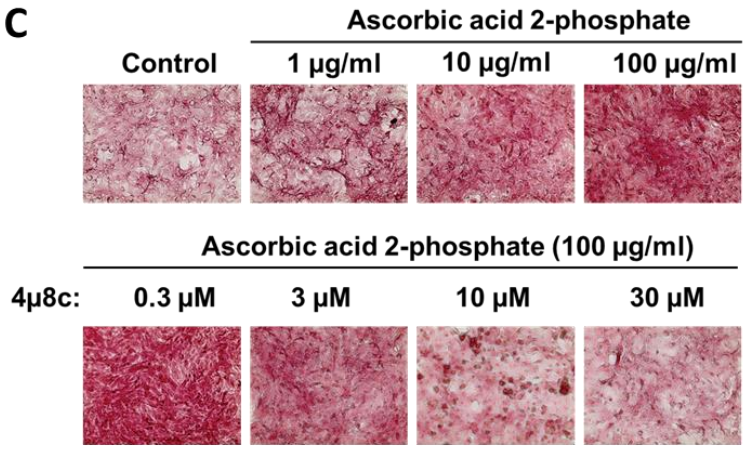

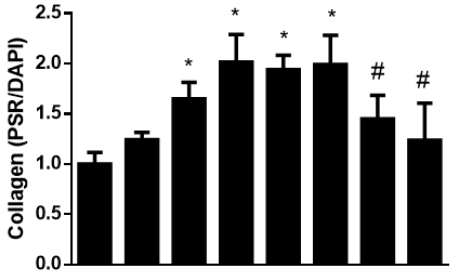

AA2P (µg/ml)	-	1	10	100				
4µ8c (µM)	-	-	-	-	0.3	3	10	30

Figure 3. Inhibition of IRE1α endonuclease activity attenuates collagen secretion from VSMCs. (A) WKY VSMCs were cultured in DMEM/F12 containing 10% FBS. Confluent cells were treated with L-ascorbic acid (100 μg/ml daily) and increasing concentrations of 4μ8c and STF-083010 for 72 h. Cells were harvested in 0.5 M acetic acid and a dot blot for Type I collagen was performed. Blots were subsequently stained with Ponceau S to visualize total protein for normalization. (B) Semi-quantitative analysis of dot blots. (C) Picrosirius Red staining of VSMCs stimulated with L-ascorbic acid-2-phosphate (AA2P) and increasing concentrations of 4μ8c. (D) Spectrophotometric measurement of eluted Picrosirius Red dye from ASMCs. Data is presented as mean ± SEM. *, $p<0.05$ vs. Vehicle; #, $p<0.05$ vs. 100 μg/ml L-ascorbic acid.

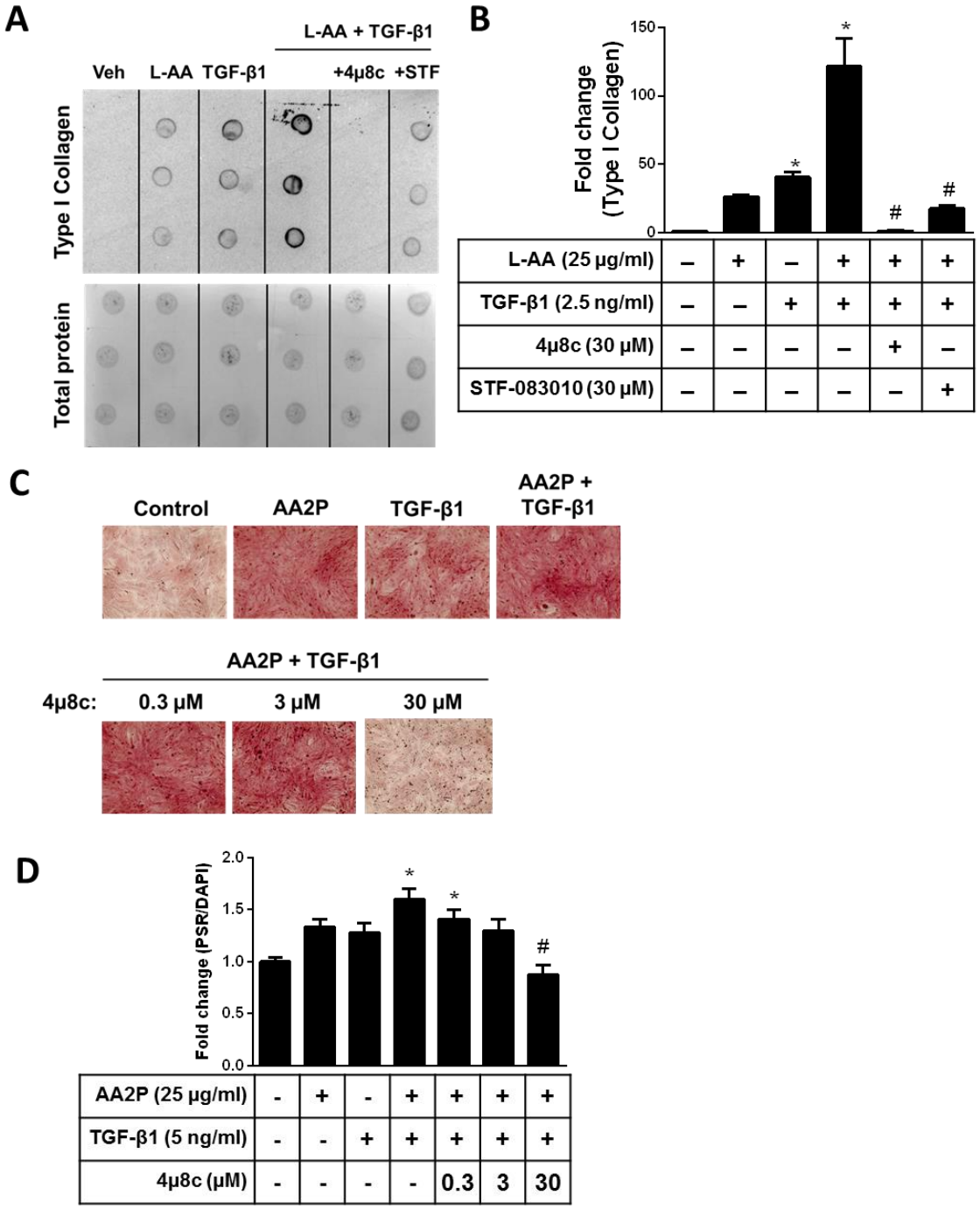
A
L-AA + TGF-β1
Veh
L-AA
TGF-β1
+4μ8c
+STF
Type I Collagen
Total protein
B
Fold change (Type I Collagen)
150
100
50
0
*
*
#
#
L-AA (25 μg/ml) – + – + + +
TGF-β1 (2.5 ng/ml) – – + + + +
4μ8c (30 μM) – – – – + –
STF-083010 (30 μM) – – – – – +
C
Control
AA2P
TGF-β1
AA2P + TGF-β1
AA2P + TGF-β1
4μ8c:
0.3 μM
3 μM
30 μM
D
Fold change (PSR/DAPI)
2.0
1.5
1.0
0.5
0.0
*
*
#
AA2P (25 μg/ml) - + - + + + +
TGF-β1 (5 ng/ml) - - + + + + +
4μ8c (μM) - - - - 0.3 3 30

E

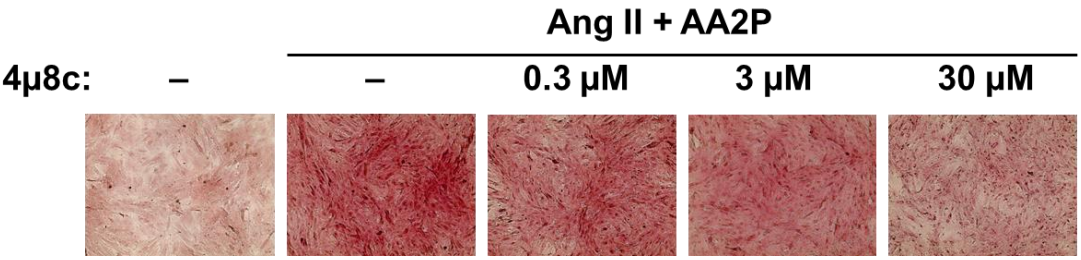

F

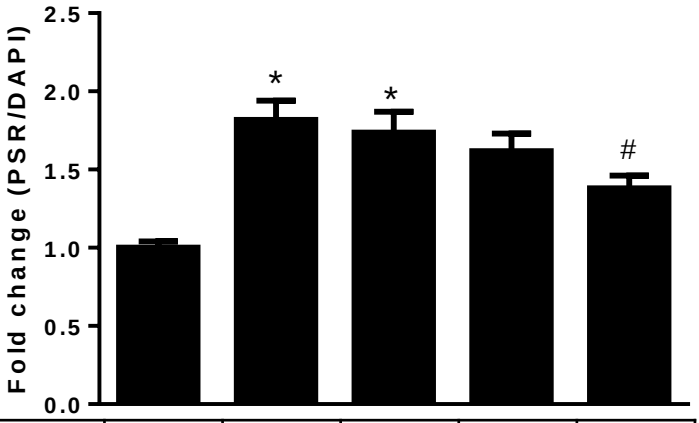

AA2P (25 μg/ml)	-	+	+	+	+
Ang II (1 μM)	-	+	+	+	+
4μ8c (μM)	-	-	0.3	3	30

Figure 4. IRE1α inhibition reduces TGF-β1- and Ang II-induced collagen synthesis in VSMCs. WKY VSMCs were cultured in DMEM/F12 containing 1% FBS. Confluent cells were treated with L-ascorbic acid (25 μg/ml) and either TGF-β1 (5 ng/ml) or Ang II (1 μM). Dot blot (A,B) and PSR assay (C,D) demonstrated that co-treatment of cells with both TGF-β1 and L-ascorbic acid resulted in an additive effect on collagen synthesis, which was repressed by 4μ8c (30 μM) and STF-083010 (30 μM). (E,F) PSR assay demonstrating the effect of combined treatment with Angiotensin II (1 μM) and AA2P (25 μg/ml) on collagen synthesis and co-treatment with 4μ8c. Data is presented as mean ± SEM. *, $p<0.05$ vs. Vehicle; #, $p<0.05$ vs. TGF-β1 (B, D) or Ang II (F) in the presence of AA2P.

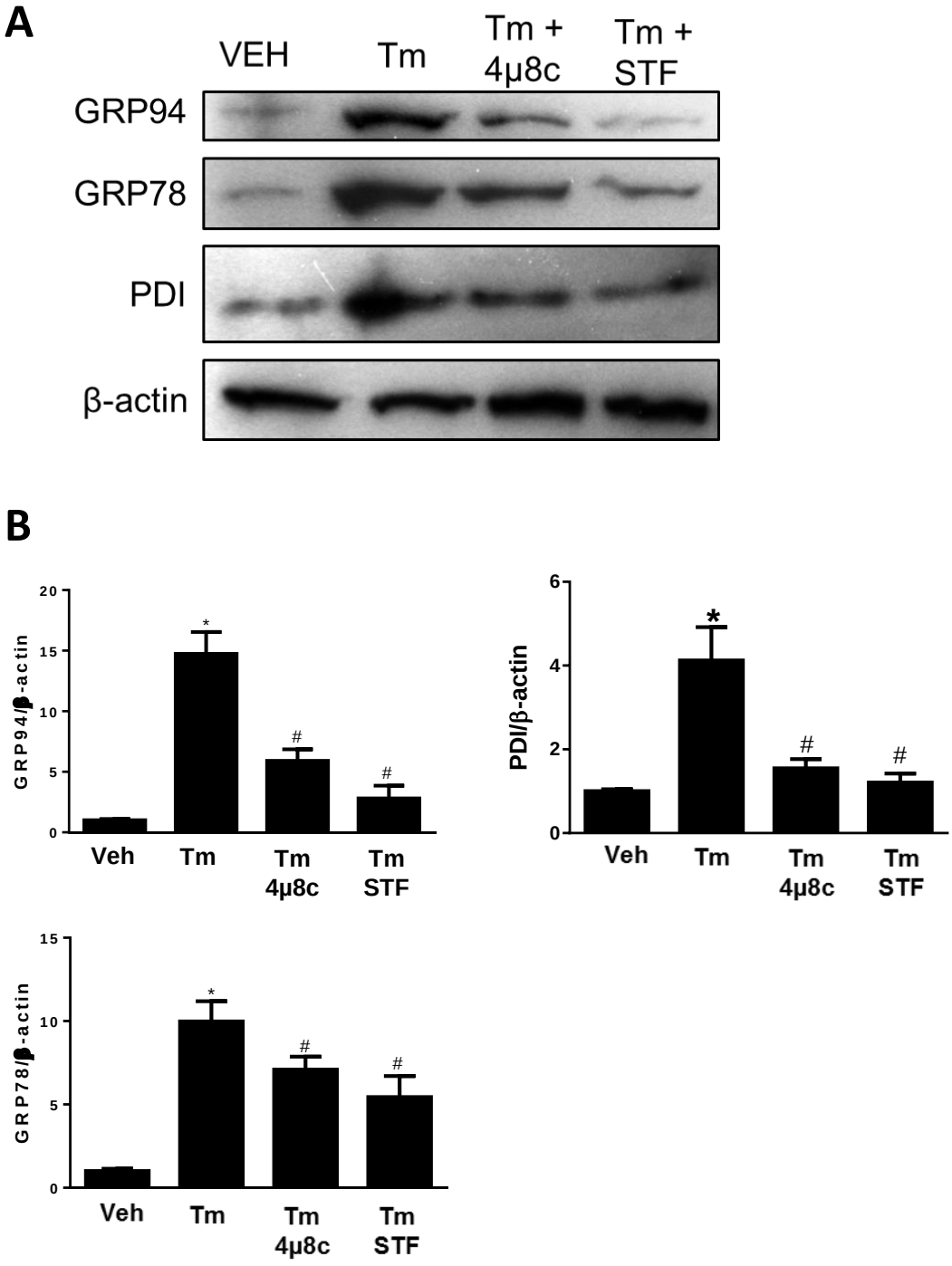
A
VEH
Tm
Tm + 4μ8c
Tm + STF
GRP94
GRP78
PDI
β-actin
B
GRP94/β-actin
PDI/β-actin
GRP78/β-actin
Veh
Tm
Tm 4μ8c
Tm STF

Figure 5. IRE1α inhibition reduces the expression of collagen-associated chaperones induced by ER stress. WKY ASMCs were treated with tunicamycin (1 μg/ml) for 24 h, with or without 4μ8c (30 μM) or STF-083010 (60 μM). (A) Immunoblotting for GRP78, GRP94, PDI and β-actin. (B) Densitometric analysis and normalization to β-actin. Data is presented as mean ± SEM. *, $p<0.05$ vs. Vehicle; #, $p<0.05$ vs. Tm.

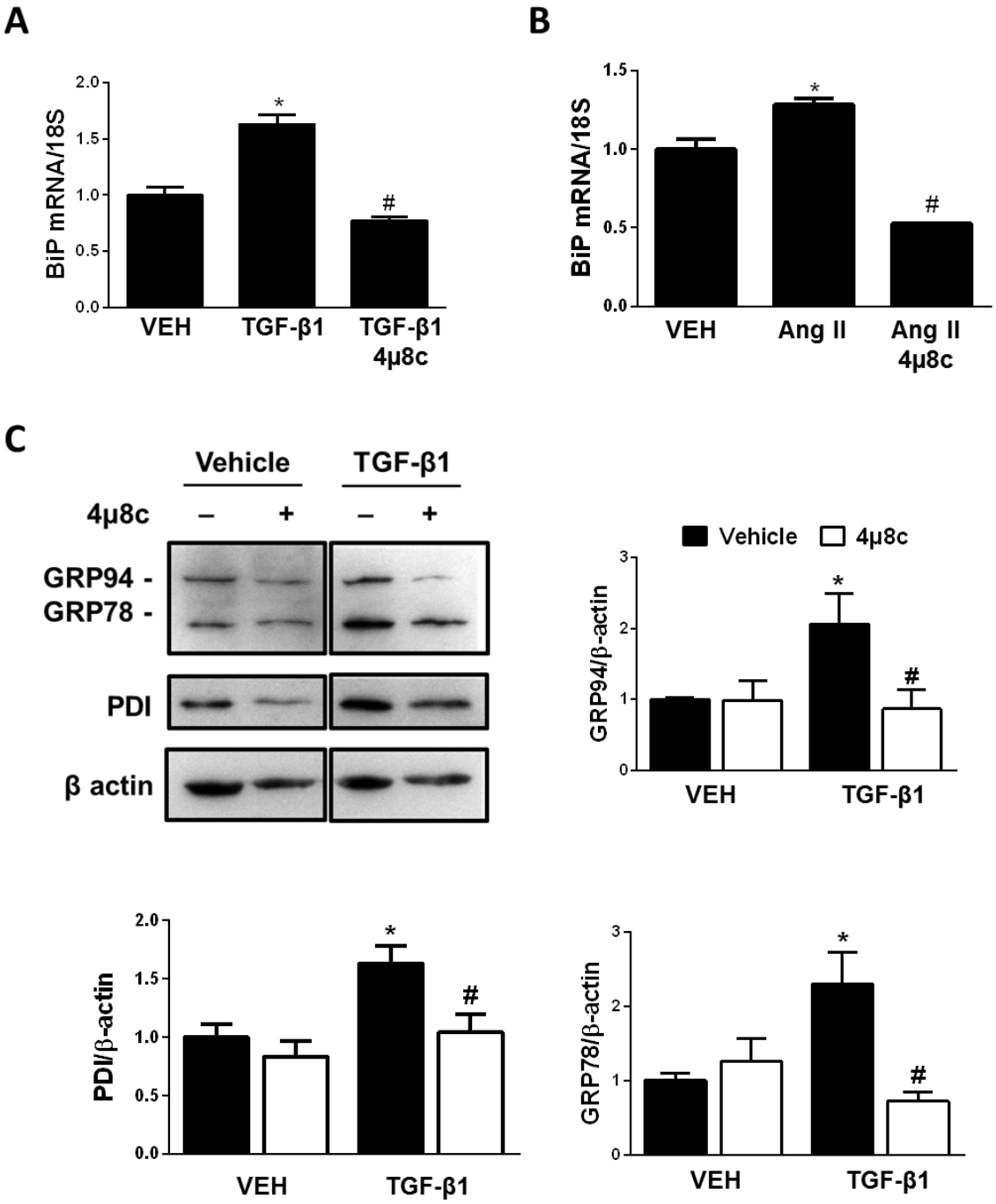
A
BiP mRNA/18S
2.0
1.5
1.0
0.5
0.0
*
#
VEH
TGF-β1
TGF-β1
4μ8c
B
BiP mRNA/18S
1.5
1.0
0.5
0.0
*
#
VEH
Ang II
Ang II
4μ8c
C
Vehicle
TGF-β1
4μ8c
–
+
–
+
GRP94 -
GRP78 -
PDI
β actin
Vehicle
4μ8c
GRP94/β-actin
3
2
1
0
*
#
VEH
TGF-β1
PDI/β-actin
2.0
1.5
1.0
0.5
0.0
*
#
VEH
TGF-β1
GRP78/β-actin
3
2
1
0
*
#
VEH
TGF-β1

Figure 6. IRE1α inhibition reduces the expression of GRP78, GRP94 and PDI under conditions of TGF-β1 or Ang II-induced ER stress. WKY VSMCs were treated with either TGF-β1 (2.5 ng/ml) or Ang II (1 μM) in the presence of AA2P (25 μg/ml) for 24 or 48 h. (A) qRT-PCR for GRP78 in WKY VSMCs treated with TGF-β1 and AA2P with or without 4μ8c (30 μM) for 24 h. (B) qRT-PCR for GRP78 in WKY VSMCs treated with Ang II and AA2P in the presence or absence of 4μ8c (30 μM) for 24 h. (C) Immunoblot for assessment of UPR marker expression after TGF-β1 treatment (5 ng/ml) for 48 h with or without 4μ8c (30 μM). Densitometric analysis and normalization to β-actin are shown. Data is presented as mean ± SEM. *, $p<0.05$ vs. Vehicle; #, $p<0.05$ vs. TGF-β1 (A) or Ang II (B).

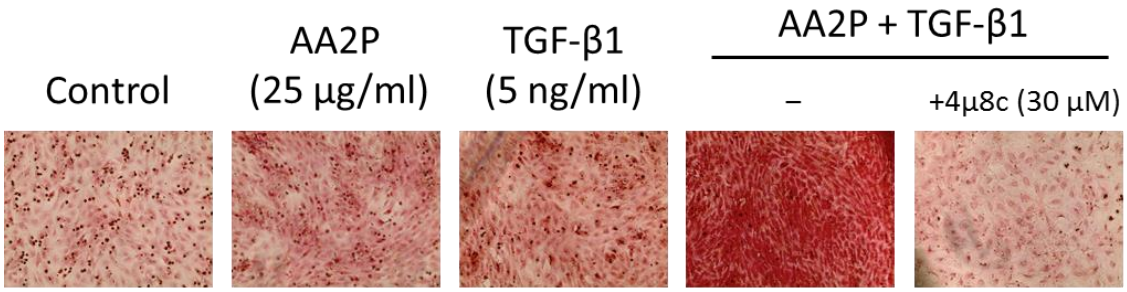

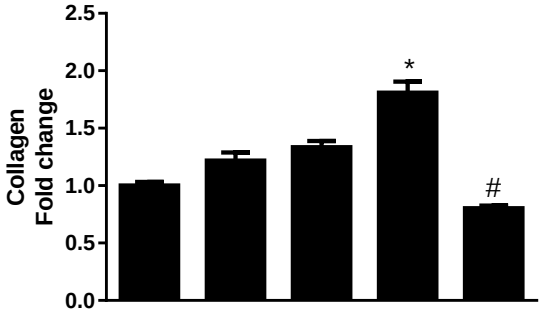

AA2P (25 µg/ml)	-	+	-	+	+
TGF-β1 (5 ng/ml)	-	-	+	+	+
4µ8c (30 µM)	-	-	-	-	+

Figure 7. IRE1 inhibition prevents collagen deposition by renal fibroblasts. Rat renal fibroblasts were treated with L-ascorbic acid-2-phosphate, TGF-β1 and 4μ8c for 72 h. Collagen production was measured by a Picro-Sirius Red assay. **, $p<0.01$.

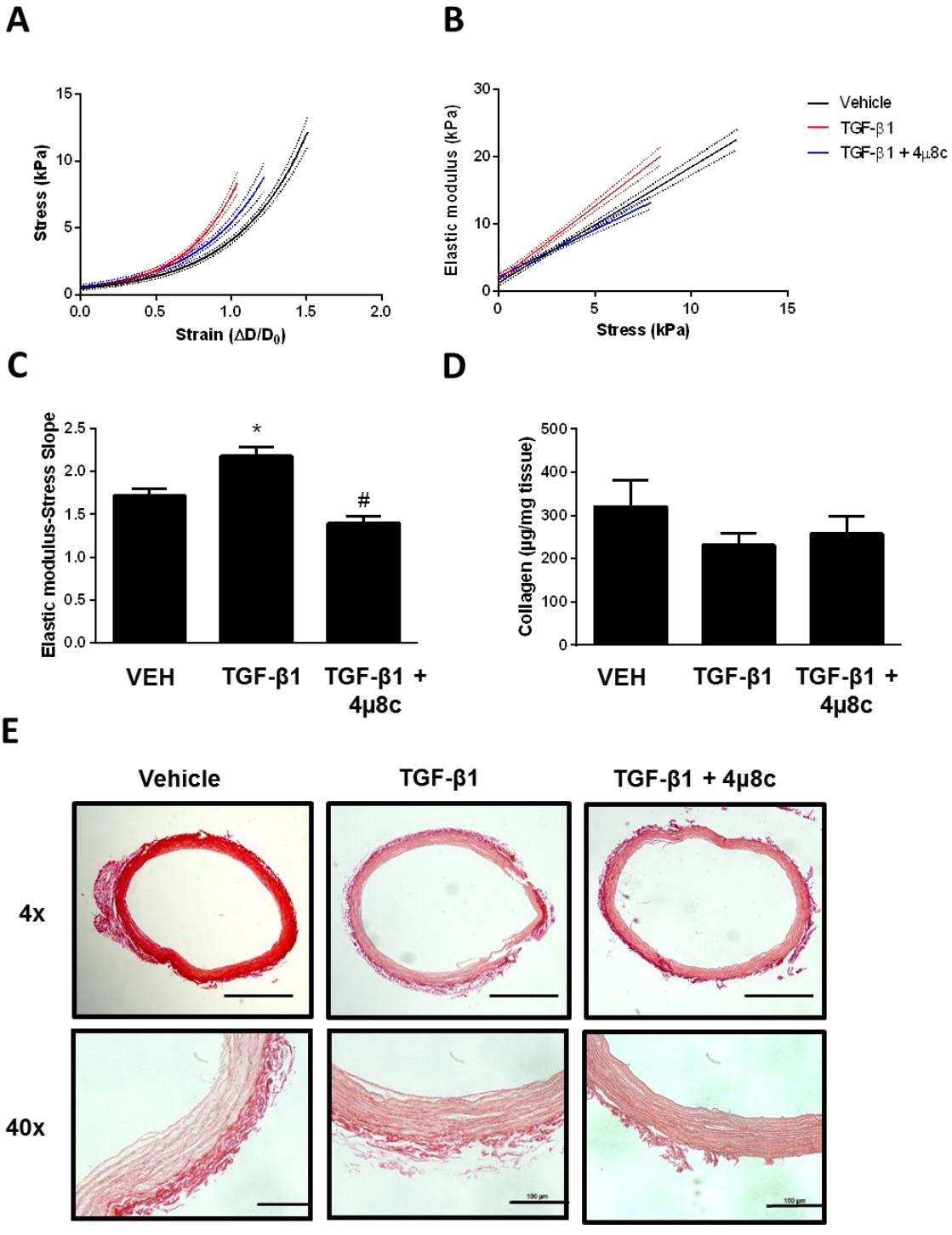
A
B
Stress (kPa)
Strain (ΔD/D0)
Elastic modulus (kPa)
Stress (kPa)
Vehicle
TGF-β1
TGF-β1 + 4μ8c
C
D
Elastic modulus-Stress Slope
Collagen (μg/mg tissue)
VEH
TGF-β1
TGF-β1 + 4μ8c
E
Vehicle
TGF-β1
TGF-β1 + 4μ8c
4x
40x

Figure 8. Inhibition of IRE1 endonuclease activity prevents TGF-β1-induced stiffening of cultured aortic rings. Aortic rings were treated with TGF-β1 (5 ng/ml) for 5 days and co-treated with 4μ8c (30 μM). Compliance was measured using a wire myograph and stress-strain curves (A) and elastic modulus-stress curves (B) were derived. The slope of the elastic modulus-stress line was calculated (C) to provide a measure of geometry-independent stiffness. TGF-β1 increased the stiffness of aortic rings while co-treatment with 4μ8c inhibited this effect. Each curve is bound by 95% prediction bands. (D) Measurement of collagen content in aortic rings by PSR assay. (E) PSR staining of fixed aortic rings and imaging at 4x and 40x magnification. Bar, 4x magnification, 500 μm; 40x magnification, 100 μm. $N \geq 4$ per treatment group. Data is presented as mean ± SEM. *, $p<0.05$

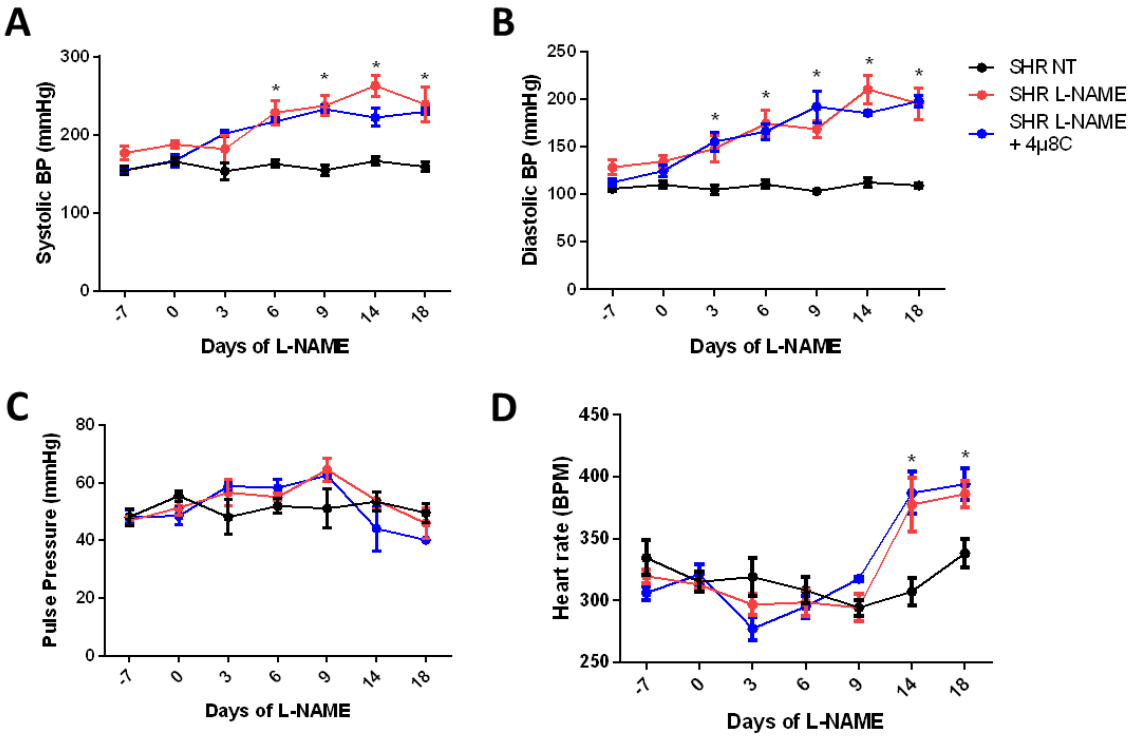
A
Systolic BP (mmHg)
300
200
100
0
-7
0
3
6
9
14
18
Days of L-NAME
B
Diastolic BP (mmHg)
250
200
150
100
50
0
Days of L-NAME
SHR NT
SHR L-NAME
SHR L-NAME + 4μ8C
C
Pulse Pressure (mmHg)
80
60
40
20
0
Days of L-NAME
D
Heart rate (BPM)
450
400
350
300
250
Days of L-NAME

Figure 9. 4μ8c does not affect blood pressure in L-NAME-treated SHRs. 12-14 week old male SHRs were implanted with radiotelemetry devices and randomized to receive vehicle, L-NAME (50 mg/L) or L-NAME and 4μ8c (2.5 mg/kg/day i.p.) for 18 days. Systolic (A), diastolic (B), pulse pressure (C) and heart rate (D) were monitored. Data is presented as mean ± SEM. *, $p<0.05$ vs. NT; #, $p<0.05$ vs. L-NAME. $N \geq 4$ per group.

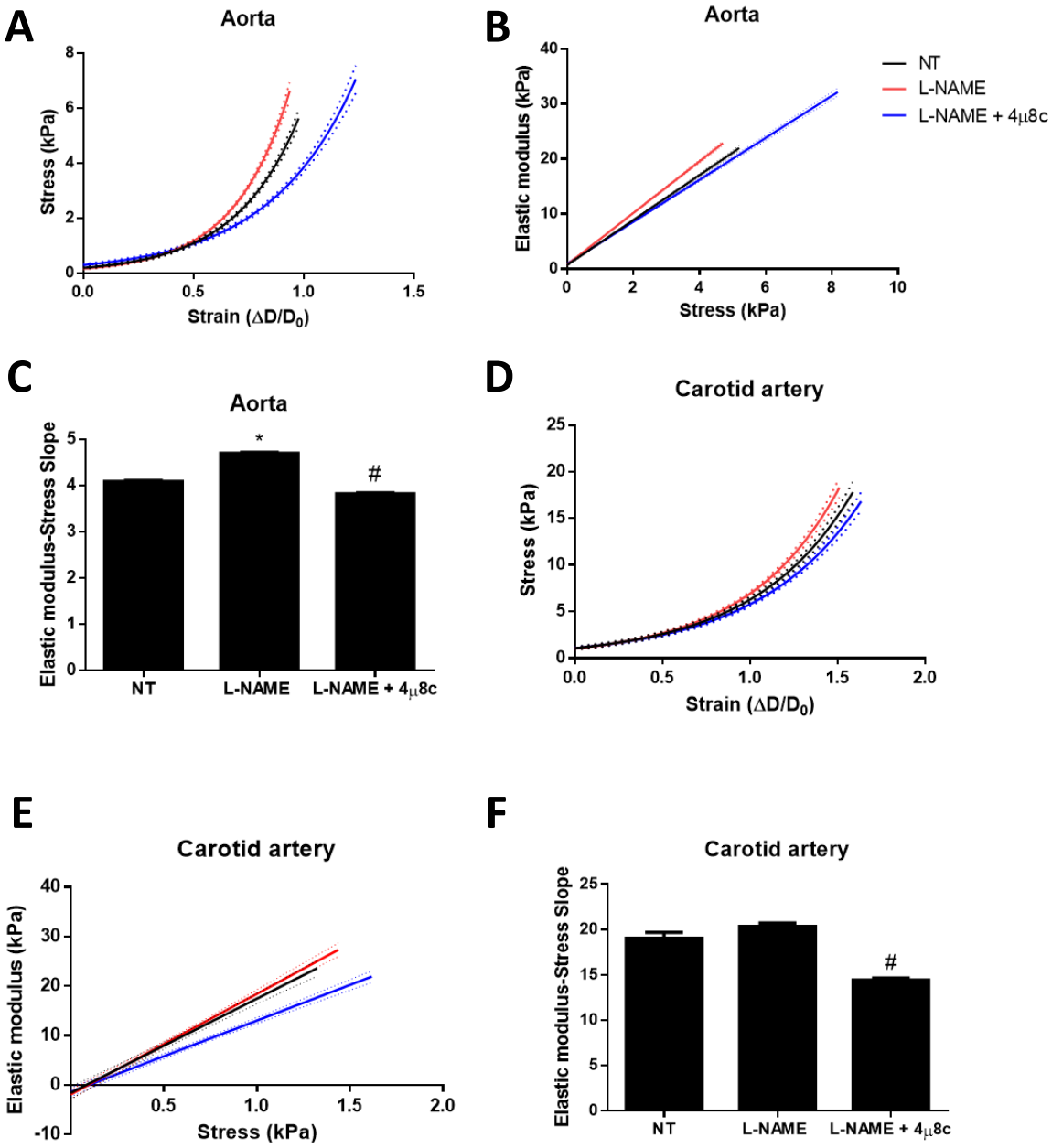
A
Aorta
Stress (kPa)
Strain (ΔD/D0)
B
Aorta
Elastic modulus (kPa)
Stress (kPa)
NT
L-NAME
L-NAME + 4μ8c
C
Aorta
Elastic modulus-Stress Slope
*
#
NT
L-NAME
L-NAME + 4μ8c
D
Carotid artery
Stress (kPa)
Strain (ΔD/D0)
E
Carotid artery
Elastic modulus (kPa)
Stress (kPa)
F
Carotid artery
Elastic modulus-Stress Slope
#
NT
L-NAME
L-NAME + 4μ8c

Figure 10. 4μ8c reduces vascular stiffening induced by L-NAME. 12-14 week old male SHRs were randomized to receive vehicle, L-NAME (50 mg/L) or L-NAME and 4μ8c (2.5 mg/kg/day i.p.) for 18 days. Aortas and carotid arteries were removed at sacrifice and compliance was measured using a wire myograph. Stress-strain curves (A,D), elastic modulus-stress lines (B,E) and the slope of the elastic modulus-stress lines (C,F) were calculated. Data is presented as mean ± SEM. *, $p<0.05$ vs. NT; #, $p<0.05$ vs. L-NAME. $N \geq 4$ per group; 2-5 segments of the thoracic aorta were analyzed per animal.

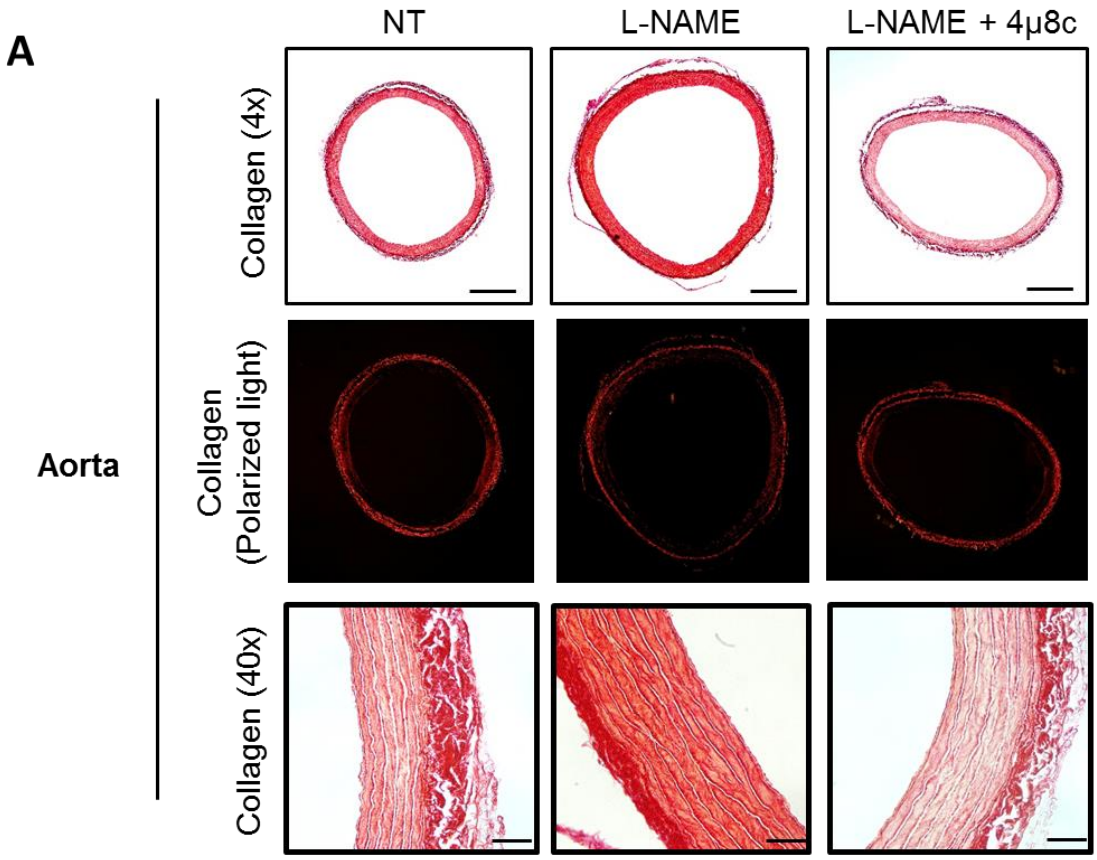
A
NT
L-NAME
L-NAME + 4µ8c
Aorta
Collagen (4x)
Collagen (Polarized light)
Collagen (40x)

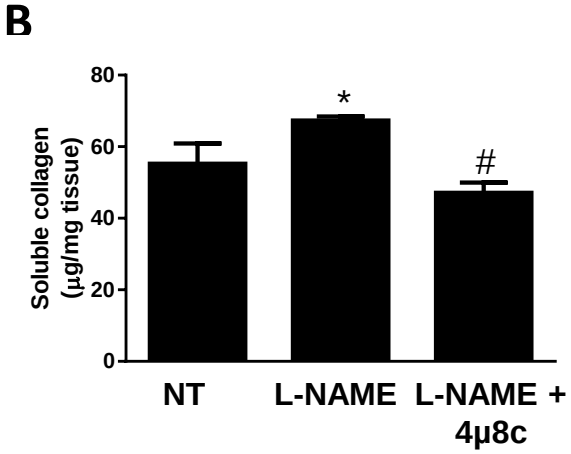
B
Soluble collagen (µg/mg tissue)
80
60
40
20
0
*
#
NT
L-NAME
L-NAME + 4µ8c

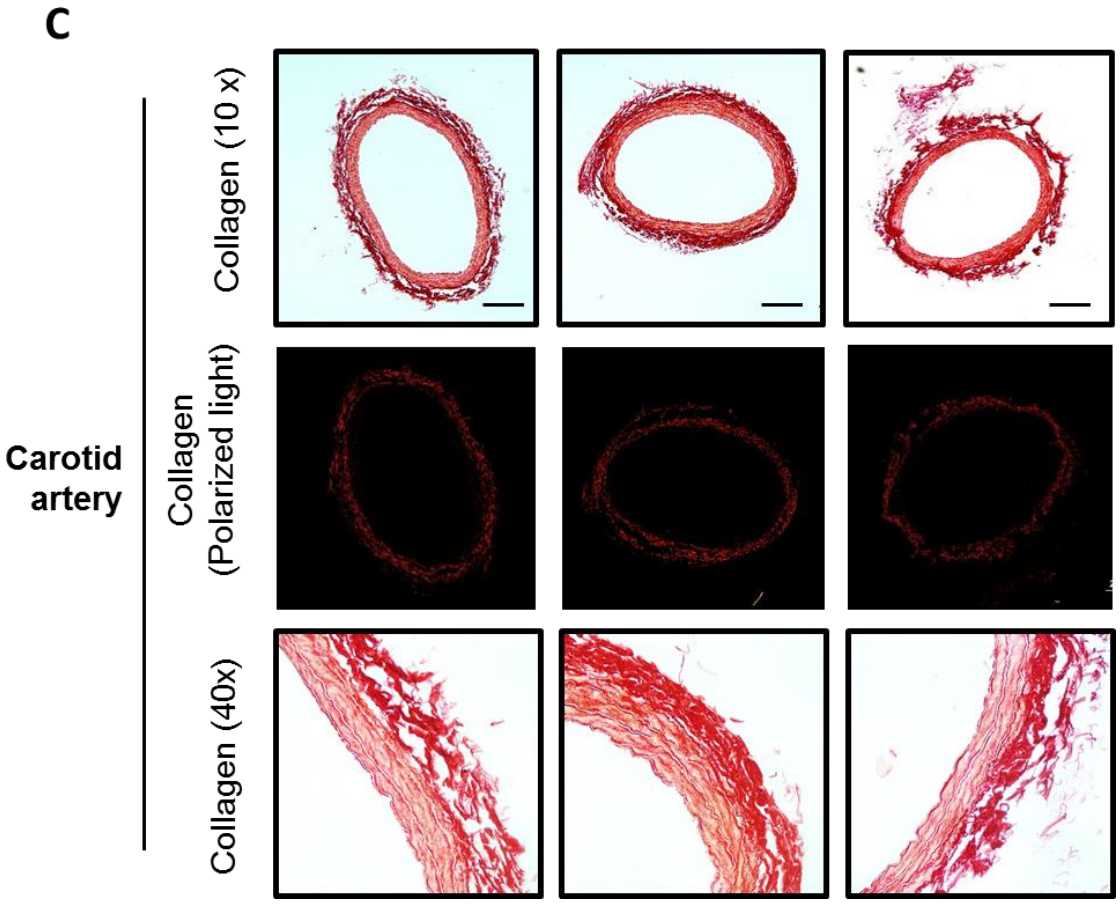
C
Carotid artery
Collagen (10 x)
Collagen (Polarized light)
Collagen (40x)
D
Collagen area density (%)
100
80
60
40
20
0
NT
L-NAME
L-NAME + 4μ8c

Figure 11. 4μ8c reduces aortic fibrosis in L-NAME-treated SHRs. 12-14 week old male SHRs were randomized to receive vehicle, L-NAME (50 mg/L) or L-NAME and 4μ8c (2.5 mg/kg/day i.p.) for 18 days. Aortas (A) and carotid arteries (C) were fixed and stained with Picrosirius Red for morphometric analysis. Bar, 4x, 500 μm; 10x, 200 μm; 40x, 50 μm. (B) PSR-based assay for determination of soluble collagen content per mg wet weight of tissue in aortic rings. (D) Collagen area density analysis of PSR-stained carotid arteries. Data is presented as mean ± SEM. *, $p<0.05$ vs. NT. #, $p<0.05$ vs L-NAME.

A

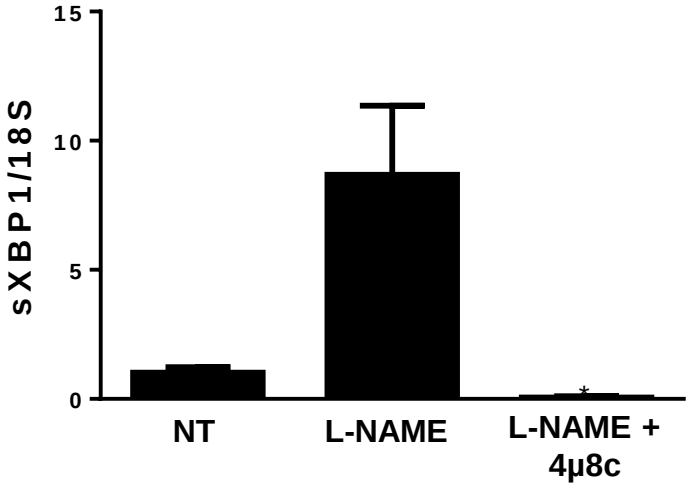
sXBP1/18S
15
10
5
0
NT
L-NAME
L-NAME +
4μ8c

B

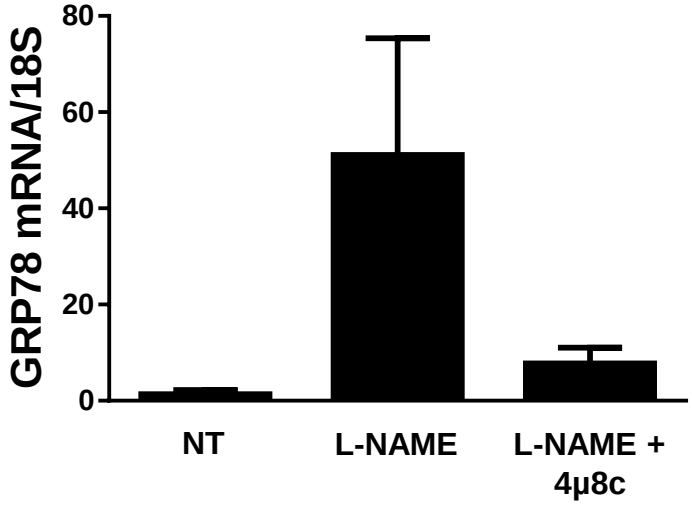
GRP78 mRNA/18S
80
60
40
20
0
NT
L-NAME
L-NAME +
4μ8c

Figure 12. Effect of 4μ8c on aortic collagen chaperone expression in L-NAME-treated SHRs. 12-14 week old male SHRs were randomized to receive vehicle, L-NAME (50 mg/L) or L-NAME and 4μ8c (2.5 mg/kg/day i.p.) for 18 days. Total RNA was extracted from flash frozen aortic tissues. qRT-PCR was used to assess relative mRNA expression of spliced XBP1 (A) and GRP78 (B). 18S was used as a housekeeping gene. Data is presented as mean ± SEM. *, $p<0.05$ vs. NT. #, $p<0.05$ vs L-NAME.

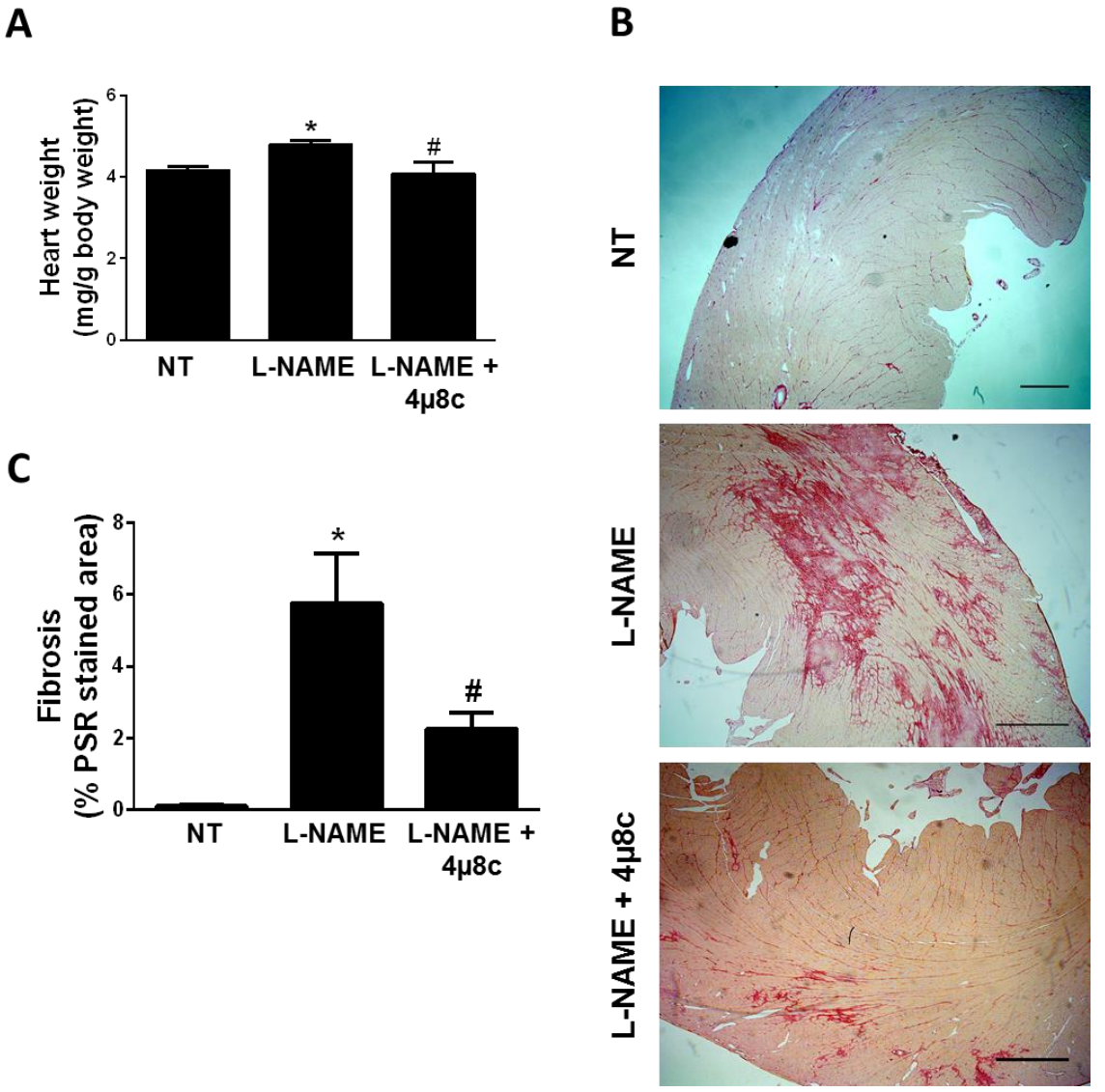
A
Heart weight
(mg/g body weight)
0
2
4
6
*
#
NT
L-NAME
L-NAME +
4μ8c
B
NT
L-NAME
L-NAME + 4μ8c
C
Fibrosis
(% PSR stained area)
0
2
4
6
8
*
#
NT
L-NAME
L-NAME +
4μ8c

Figure 13. 4μ8c reduces cardiac fibrosis in L-NAME-treated SHRs. 12-14 week old male SHRs were randomized to receive vehicle, L-NAME (50 mg/L) or L-NAME and 4μ8c (2.5 mg/kg/day i.p.) for 18 days. (A) Cardiac hypertrophy measured using heart weight to body ratio. (B) PSR staining of transverse heart sections. (C) Quantification of PSR-stained area in heart tissue. Bar, 500 μm. Data is presented as mean ± SEM. *, $p<0.05$ vs. NT. #, $p<0.05$ vs L-NAME.

Table 1. Effect of 4μ8c in SHR/L-NAME model.

	SHR NT	SHR/L-NAME	SHR/L-NAME + 4μ8c
Body weight (g)	339.8±6.3	289.3±4.5 *	290.8±11.0 *
Heart weight (mg/g BW)	4.126±0.052	4.751±0.099 *	4.085±0.275 #
Aorta morphology			
Lumen area (mm^2)	1.668±0.071	2.075±0.137	1.968±0.157
Medial cross-sectional area (mm^2)	0.438±0.056	0.765±0.063 *	0.598±0.049 #
Media-lumen ratio	0.309±0.029	0.346±0.008	0.312±0.009
Intimal-Medial thickness (μm)	91.3±3.3	126.8±5.8 *	114.0±7.8
Carotid artery morphology			
Lumen area (mm^2)	0.370±0.012	0.340±0.010	0.360±0.027
Medial cross-sectional area (mm^2)	0.146±0.011	0.141±0.001	0.134±0.012
Media-lumen ratio	0.395±0.019	0.414±0.010	0.371±0.005 #
Intimal-Medial thickness (μm)	62.1±3.6	62.2±0.5	55.1±1.0 #

*, $p<0.05$ vs. SHR NT; #, $p<0.05$ vs. SHR/L-NAME

A

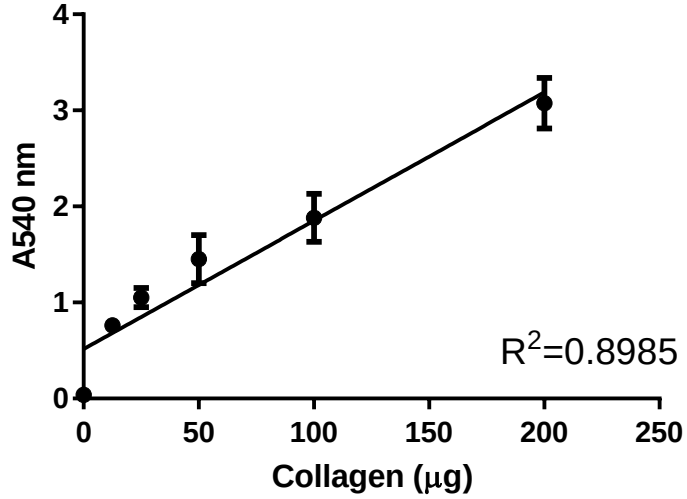
A540 nm
Collagen (μg)
R2=0.8985
0
1
2
3
4
0
50
100
150
200
250

B

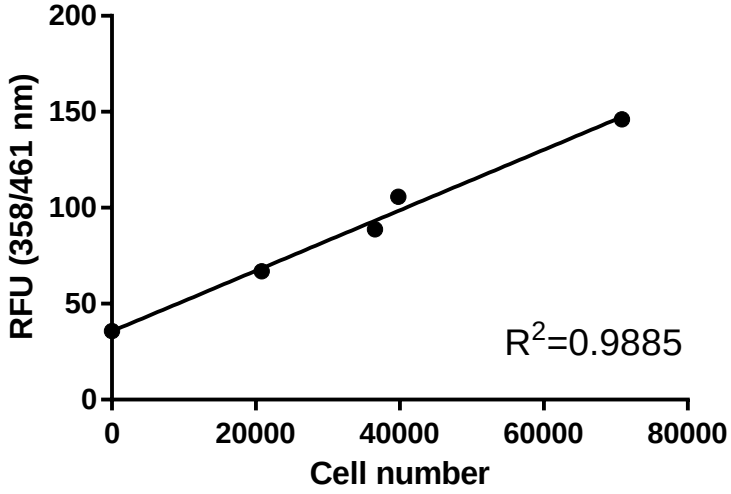
RFU (358/461 nm)
Cell number
R2=0.9885
0
50
100
150
200
0
20000
40000
60000
80000

Figure S1. Standard curves for Picro-Sirius Red assay. (A) Dilutions of a Type I collagen were loaded on a 96-well plate, dried overnight and stained with PSR. The dye was eluted and absorbance at 540 nm was measured. (B) WKY ASMCs were seeded on a 96-well plate at various densities, fixed and stained with DAPI. DAPI fluorescence was measured on a spectrofluorometer at 358/461 nm.

4. DISCUSSION

4.1 Effect of IRE1α inhibition on collagen secretion from VSMCs

The aim of this study was to determine if the inhibition IRE1α endonuclease activity in VSMCs reduces the secretion of collagen in the presence of profibrotic stimuli. Since VSMCs are an important source of collagen during the progression of vascular fibrosis, we hypothesized that inhibition of IRE1α would attenuate the development of vascular fibrosis and improve vessel compliance. We began by testing this hypothesis using the chemical inhibitor of IRE1α endonuclease activity, 4μ8c or STF-083010, in an in vitro model of primary rat VSMCs. We first demonstrated that these two compounds are able to block IRE1α endonuclease activity in VSMCs. Using tunicamycin, TGFβ1 and Ang II to induce XBP1 splicing, co-treatment with 4μ8c or STF-083010 was observed to inhibit the formation of the spliced transcript variant of XBP1. This was measured by both qRT-PCR and RT-PCR followed by agarose gel electrophoresis.

Next, we tested our core hypothesis by inducing collagen synthesis in VSMCs using L-ascorbic acid, TGF-β1 or Ang II, and tested the ability of 4μ8c and STF-083010 to inhibit this process. While L-ascorbic acid and its derivative L-ascorbic acid-2-phosphate were sufficient to induce collagen synthesis in the presence of 10% FBS, TGF-β1 and Ang II required the presence of L-ascorbic acid. We observed that at maximum doses of 4μ8c (30 μM) and STF-083010 (60 μM), collagen synthesis was inhibited regardless of the stimulus used. Since two structurally different inhibitors were used, this minimizes the probability that the observed inhibition was due to an off-target effect.

To elucidate the mechanisms by which IRE1α regulates collagen synthesis, we assessed the expression of ER resident chaperones that have been shown to interact with collagen during its biosynthesis. By qRT-PCR and Western blotting, we observed that the expression of GRP78, GRP94 and PDI were induced in ER stress conditions and lowered by IRE1α inhibition. These collagen-associated chaperones have been identified as targets of XBP1s in other professional secretory cells such as pancreatic β-cells and plasma cells (65). The collagen-specific chaperone HSP47, however, was not affected by IRE1α inhibition. Taken together, these results suggest that a potential mechanism by which IRE1α inhibition lowers collagen synthesis is by reducing the availability of chaperones that are necessary for the proper folding of the procollagen triple helix.

There is evidence that the loss of ER-resident chaperones is associated with reduced collagen production. Studies have been published that directly examine the role of calreticulin, an ER chaperone and a target of spliced XBP1, in collagen biosynthesis. Van Duyn Graham et al. demonstrated in calreticulin-deficient MEFs that collagen molecules remain trapped in the ER and are unable to be secreted and incorporated into the ECM (91). Calreticulin has also been shown to be necessary for the TGF-β1-induced production of collagen (99). Similarly, the deletion of HSP47 causes the accumulation of immature type I collagen within the ER, leading to ER stress and apoptosis (100–102). Since HSP47 has been observed to form heterocomplexes with GRP78, GRP94 and procollagen during the collagen maturation process, it can be hypothesized that similar effects would be observed if GRP78 and GRP94 are downregulated (103). Consistent with our observations in VSMCs, the chemical chaperone 4-PBA has also been shown to

inhibit collagen production in fibroblasts while simultaneously lowering the expression of ER stress markers (34,75,104,105). Although this is seemingly paradoxical, since chemical chaperones would be hypothesized to aid rather than inhibit the folding of procollagen, it is possible that they are not able to compensate for the more intricate folding processes that the endogenous chaperones offer.

Heindryckx et al. recently published a study that examined a very similar hypothesis to ours (88). They demonstrated, in human fetal lung fibroblasts, that inhibition of IRE1α with 4μ8c prevented myofibroblast differentiation and collagen synthesis in response to TGF-β1. It was shown that IRE1α inhibition prevented the degradation of miR-150, a microRNA target of the IRE1α endonuclease. miR-150 targets the transcription factors c-Myb and SP1, which regulate the expression of α-SMA and collagen I, respectively. Furthermore, inhibition of XBP1 splicing resulted in decreased expansion of the ER, reducing the capacity of the cells to produce and fold ECM proteins.

A caveat of IRE1α inhibition is that by blocking the adaptive processes of the cell to restore homeostasis, ER stress may actually increase and render the cell more susceptible to apoptosis. Indeed, a recent study by Walter et al. demonstrated that knockdown of IRE1α resulted in an earlier onset of ER stress-induced cell death due to the abrogation of the spliced XBP1-mediated pro-survival response (106). In a similar manner, the deletion of HSP47 (100) or calreticulin (91) results in the retention of collagen in the ER, leading to subsequent ER stress and apoptosis. There is much interest regarding the role of IRE1α as a cell fate regulator due to its ability to initiate both pro-survival and pro-apoptotic responses (62,64,107). During the pro-survival phase, the endoribonuclease domain of

IRE1α can also target the degradation of the mRNA of ER-translocating proteins through regulated IRE1-dependent decay (RIDD). However, it has been observed that under prolonged ER stress, IRE1α begins degrading the mRNA of UPR target genes such as GRP78 which in effect ends the adaptive response and promotes an increase in ER stress (64). IRE1α also begins degrading anti-Caspase 2 microRNAs, resulting in an increase in Caspase 2 expression and initiation of ER stress-induced apoptosis (63).

4.2 Effect of IRE1α inhibition on vascular stiffening

The overall aim of this project was to determine the role of the IRE1α pathway in the development of vascular stiffening during hypertension. The fibrotic remodelling of elastic arteries is one mechanism by which vascular stiffening can develop. Up to this point, we have demonstrated that inhibition of the IRE1α endonuclease prevents the production of collagen by VSMCs. We then sought to test our hypothesis using an ex vivo and an in vivo model of vascular stiffening.

We first tested our hypothesis using an ex vivo organ culture model of aortic rings. This model was adapted from vascular calcification models that were previously described (97,108). Instead of supplementing the medium with phosphate to induce calcification, we supplemented it with L-ascorbic acid and TGF-β1 to stimulate fibrosis in a similar manner to our in vitro work. After a 5 day incubation period, the vessels were mounted on a wire myograph for assessment of stiffness. We observed that TGF-β1 induced vascular stiffening in these aortic rings, as demonstrated by the leftward shift of the stress-strain relationship and increase in the incremental elastic modulus, while co-

treatment with 4μ8c or STF attenuated this. However, we did not observe any differences in total collagen content between the groups. Preliminary histological analysis with PSR staining suggested that the distribution of the collagen in the vessel wall may be different between groups. Control aortic rings displayed a normal collagen-rich adventitia and little collagen in the medial layer. On the contrary, TGF-β1-treated vessels seemed to show disintegration of the adventitia while collagen content in the media was increased. The increase in medial collagen content could reflect the ability of TGF-β1 to induce collagen synthesis in VSMCs, as observed in vitro. This raises further questions about the relative contribution of the adventitia and media to the overall stiffness of the blood vessel. It is possible that fibrosis in the medial layer has a greater impact on vascular stiffness than an equivalent increase in collagen content within the adventitia. This could be due to the strong adhesions that are formed between the collagen fibers and the VSMCs (14). Further experiments need to be performed to test this hypothesis.

We next tested our hypothesis using the SHR/L-NAME model of vascular stiffening. In this model, 12-14 week old SHRs are administered a low dose of the nitric oxide synthase inhibitor L-NAME to induce malignant hypertension. This animal model has been shown to develop vascular stiffening, as measured in vivo by PWV and β-index (109). In addition, these animals also develop renal damage (110–112) and cardiac damage (113,114) associated with the fibrotic remodelling of these organs. We sought to determine whether systemic administration of the IRE1α inhibitor 4μ8c would prevent the development of fibrosis in this model. Animals were implanted with radiotelemetry devices for continuous measurement of blood pressure. This provides a more accurate

measurement of blood pressure compared to other methods such as tail-cuff because the animals are conscious and stress caused by handling and restraint are minimized. As expected, L-NAME increased both systolic and diastolic blood pressures in the SHR. Daily injections of 4μ8c had no effect on the blood pressure elevation induced by L-NAME. This enabled us to rule out blood pressure as a confounder in any effects that were observed in terms of vascular stiffness or fibrosis. Interestingly, heart rate was elevated in the L-NAME-treated animals at Day 14 and Day 18. This is consistent with the work of Souza et al., who found that L-NAME induces cardiac sympathetic overactivity and decreases baroreflex sensitivity (115).

Our primary endpoint in this study was vascular stiffness as measured by wire myography. Aortas and carotid arteries were collected at sacrifice and mounted on a wire myograph under maximally relaxed conditions. We observed an increase in vascular stiffness with L-NAME treatment in the aorta but not the carotid artery of the SHRs. However, in both vessels, co-treatment with 4μ8c reduced vascular stiffness even below the level of the non-treated control. We observed an increase in medial cross-sectional area, intimal-medial thickness, and collagen content in L-NAME aortas, which was reduced by 4μ8c. In the carotid arteries, collagen density was elevated in the L-NAME aortas and lowered by 4μ8c. A potential explanation for this is that inhibition of IRE1α reduces the normal turnover of matrix proteins in the L-NAME-treated and non-treated SHR, as we had observed in our in vitro data. In addition to the difference in absolute collagen content between the groups, the organization of the collagen in both the media and the adventitia appears denser in the L-NAME aortas compared to the non-treated or

4μ8c-treated aortas. The adventitial collagen in the latter two groups appears more disorganized, which can reduce the tensile strength of the aorta and hence reduce stiffness (12,116). This has been observed in humans, where the weakened vessel wall in abdominal aortic aneurysms was shown to have more disorganized collagen fibers compared to normal segments of the aorta (116). Because ECM remodelling involves the simultaneous destruction of the existing matrix and the deposition of new matrix proteins, it is possible that under IRE1α blockade by 4μ8c, matrix destruction by MMPs is allowed to continue while matrix production is inhibited. The overall result is a net degradation of the ECM. These results suggest that IRE1α endonuclease activity is required for the development of vascular stiffening in this model.

The data presented here is the first to examine the intrinsic vascular stiffness of vessels in the SHR/L-NAME model. It expands upon the work done by Isabelle et al., which characterized the development of vascular stiffening in the SHR/L-NAME model using pulse wave velocity and β-index measurements (109,117). Although these measurements do have clinical value, they are also dependent on many factors including blood pressure and vascular tone. Since our hypothesis is largely based on changes in the composition of the vessel wall, we decided to use the wire myograph to measure vascular compliance.

Our work also expands upon the study by Spitler and Webb, which was the first to examine the role of ER stress in vascular stiffening (58). In their study, 4-PBA and TUDCA were shown to reduce vascular stiffening and fibrosis in an Ang II-infusion model. This was accompanied by a reduction of ER stress markers and apoptosis in VSMCs. VSMC apoptosis has been previously shown to promote collagen synthesis by

releasing pro-fibrotic cytokines such as IL-6 (74). It was thus proposed that inhibition of VSMC apoptosis with the chemical chaperones was able to prevent the development of vascular fibrosis by reducing the secretion of these pro-fibrotic factors. As previously discussed, this may seem counterintuitive to our own hypothesis that the levels of molecular chaperones present in the ER is positively associated with collagen output. However, by alleviating the ER stress in these cells, 4-PBA and TUDCA is also indirectly downregulating the activation of the three UPR pathways, including IRE1-XBP1s. It is also possible that 4-PBA and TUDCA cannot compensate for the more complex folding processes involved in the maturation of procollagen.

A limitation of our animal model was that the L-NAME treatment did not induce a robust aortic stiffening or fibrosis response in the SHRs. Although there was a statistically significant increase in vascular stiffness and collagen content, the effect size was only 10-20%. This finding is consistent with the recently published article by Isabelle et al. that studied the changes in aortic structure and composition in the SHR/L-NAME model (117). It would therefore be valuable to test the hypothesis in other models of vascular stiffening such as the Ang II infusion model used in either mice (118,119) or rats (58). Prolonging the treatment period may also increase the effect size, but with the risk of increased mortality. Furthermore, it would be beneficial to measure the levels of newly synthesized collagen as opposed to the total collagen in the vessels. This could be accomplished using heavy water labelling to monitor protein turnover rates in the aorta.

Although the changes in vascular structure and composition were less pronounced than we had expected, the cardiac fibrosis that developed in the SHR/L-NAME model was

very robust. Fibrosis was observed in both the left and right ventricles, which was reduced in the animals receiving 4μ8c. One possible explanation for this is that the improved vascular stiffness in the 4μ8c-treated animals led to reduced cardiac afterload and consequently decreased cardiac hypertrophy. However, in vivo arterial stiffness, using either PWV or β-index, was not measured in this study and thus we cannot draw conclusions about whether 4μ8c treatment altered these parameters. Other explanations for the reduced cardiac fibrosis include reduced inflammation or, consistent with our in vitro work, reduced collagen secretion by cardiac fibroblasts.

4.3 Development of methods for measuring collagen synthesis

One the challenges that was encountered during this project was finding a method to reliably measure the amount of collagen produced by the VSMCs. Western blotting was initially used, but the poor solubility of collagen at physiological pH made it difficult to separate on an SDS-PAGE gel. Furthermore, the Type I collagen antibody that was used only recognizes the native form of collagen and does not react with the heat-denatured molecule. We thus developed two methods for measuring collagen synthesis in order to test our hypothesis. The first method was a dot-blot technique adapted from Rodriguez et al. (120). Cells were scraped into 0.5 M acetic acid and briefly sonicated in order to solubilize the collagen. The lysate was blotted directly onto a nitrocellulose membrane, and a standard immunoblotting protocol was then followed. This dot-blot method allowed us to overcome the aforementioned issues with detecting collagen by a traditional western blot. However, like a western blot, the dot-blot is semi-quantitative and at best only offers an estimation of the relative amount of collagen in each treatment group. We thus sought

to develop and use a more quantitative method to measure collagen. Our PSR-based colorimetric assay was adapted from the method described by Xu et al (95). An additional step was added to the original protocol in which the cells were stained with DAPI and detected with a fluorescent plate reader in order to provide a measurement of cell number.

4.4 Clinical implications

The current therapeutic options for vascular stiffening and isolated systolic hypertension are limited to standard antihypertensive agents and lifestyle changes. The recent SPRINT trial demonstrated that setting a SBP target of less than 120 mmHg resulted in fewer cardiovascular events and mortality compared to a target of 140 mmHg, regardless of age (121). Patients with ISH tend to be more resistant to antihypertensive treatments because the hypertension is driven by aortic stiffness (8). Thus, the development of more specific treatments that target vascular stiffening may be warranted. Several clinical trials have examined the effects of anti-hypertensive drugs on vascular stiffness. Angiotensin converting enzyme (ACE) inhibitors, angiotensin receptor blockers (ARBs) and calcium channel blockers (CCBs) seem to be the most promising agents to reduce aortic stiffness (122,123). However, their mechanism of action may be due to the reduction of pressure wave reflections as a result of their vasodilatory effects on the peripheral vessels, rather than an alteration in the compliance of the aortic wall. Longer term treatments are required to assess the effect of these treatments on aortic structure and compliance.

Our current study attempts to unravel the molecular mechanisms that are involved in the fibrotic remodelling of blood vessels. We demonstrated that the IRE1α pathway is

required for collagen synthesis from VSMCs and plays a role in the development of vascular stiffening and end-organ damage in vivo. Whether or not 4μ8c or another IRE1α inhibitor can be used clinically for the treatment of vascular stiffness remains to be seen. Sunitinib and Sorafenib are the only IRE1α inhibitors that are FDA approved for clinical use in treating various cancers (124). It is important to note that these drugs are broad spectrum receptor tyrosine kinase inhibitors and were not approved on the basis of their capacity to block IRE1. Vascular stiffening is a chronic process that takes place virtually over a lifetime. Thus, long term prophylactic treatment with an IRE1α inhibitor may not be practical due to the requirement of IRE1α for normal physiological functions such as insulin production by pancreatic β cells (125). The results presented here can be better translated to other types of tissue fibrosis that develop more rapidly, such as the fibrosis that occurs in the heart, lung, kidneys and liver. For example, cardiac fibrosis can develop within days after a myocardial infarction, and thus this is a setting where acute inhibition of IRE1α can be useful.

4.5 Future Directions

The data presented here demonstrate that inhibition of IRE1α endonuclease activity reduces collagen synthesis in VSMCs and renal fibroblasts. We observed that inhibition of IRE1α also leads to a reduced expression of chaperones involved in collagen biosynthesis such as GRP78, GRP94 and PDI. Although this provides preliminary insight into the potential mechanisms by which IRE1α regulates collagen synthesis, additional work can be performed to more specifically delineate these mechanisms.

To strengthen the data obtained using 4μ8c and STF-083010, we are currently testing the use of CRISPR/Cas9 gene editing technology to generate IRE1α and XBP1 knock-out VSMCs. CRISPR consists of a Cas9 endonuclease that is complexed with a guide RNA (gRNA) containing a 20 nucleotide sequence specific to the gene being targeted. Cells are transfected with plasmids that contain the components required to form a Cas9-gRNA complex. The Cas9-gRNA complex then binds to the complementary sequence in the genomic DNA. If sufficient homology exists the gRNA and the target gene, the Cas9 enzyme will cleave the DNA to create a double strand break (DSB). This DSB can then be repaired by either the Non-Homologous End Joining (NHEJ) pathway or the Homology Directed Repair (HDR) pathway. Our system largely uses the NHEJ repair pathway, which involves the insertion or deletion of nucleotides at the DSB site as the strands are re-ligated. The result is the generation of mutations that can lead to amino acid substitutions, deletions, insertions, or frameshift mutations leading to premature stop codons.

To test the hypothesis that IRE1α inhibition reduces collagen synthesis due to a decrease in the expression of collagen-folding chaperones, we can also overexpress these chaperones in the VSMCs to determine if collagen secretion is rescued. The rationale is that while IRE1α inhibition decreases the endogenous expression of collagen-folding chaperones, cells with a higher baseline expression of these chaperones may be able to restore collagen synthesis even under IRE1α blockade. Loss-of-function experiments can also be performed by using CRISPR/Cas9 or RNA interference to generate stable knockout cell lines of the various collagen chaperones of interest. The goal of these

experiments is to identify the chaperones that are crucial in the collagen biosynthesis pathway and those that are expendable.

5. CONCLUSIONS

In this thesis, we demonstrate that the IRE1α pathway of the UPR is required for the secretion of collagen from VSMCs and other matrix-producing cells such as renal fibroblasts. We also demonstrate that IRE1α plays a role in the development of vascular stiffening and fibrosis in a model of malignant hypertension. Inhibition of the IRE1α endonuclease resulted in decreased vascular stiffness and cardiac damage in this model without an alteration of blood pressure. Although we cannot conclude on the precise mechanisms by which the IRE1α pathway regulates collagen secretion, we observed that the inhibition of the IRE1α pathway leads to a downregulation in the expression of chaperones known to interact with collagen in its biosynthetic pathway. While chronic administration of an IRE1α inhibitor in a clinical setting might be unrealistic due to the requirement of the IRE1α pathway for normal homeostatic functions, acute treatments in cases where fibrosis is developing rapidly is a potential avenue for the expansion of this research.

6. REFERENCES

1. Schmieder RE. End Organ Damage In Hypertension. Dtsch Ärztebl Int. 2010 Dec;107(49):866–73.

2. VanDeVoorde RG, Mitsnefes MM. Hypertension and CKD. Adv Chronic Kidney Dis. 2011 Sep;18(5):355–61.

3. Messerli FH, Williams B, Ritz E. Essential hypertension. The Lancet. 2007 Aug 24;370(9587):591–603.

4. Chow CK, Teo KK, Rangarajan S, Islam S, Gupta R, Avezum A, et al. Prevalence, awareness, treatment, and control of hypertension in rural and urban communities in high-, middle-, and low-income countries. JAMA. 2013 Sep 4;310(9):959–68.

5. Government of Canada SC. High blood pressure, 2013 [Internet]. 2014 [cited 2017 Jan 3]. Available from: http://www.statcan.gc.ca/pub/82-625-x/2014001/article/14020-eng.htm

6. Bavishi C, Goel S, Messerli FH. Isolated Systolic Hypertension: An Update After SPRINT. Am J Med. 2016 Dec;129(12):1251–8.

7. Franklin SS, Jacobs MJ, Wong ND, L'Italien GJ, Lapuerta P. Predominance of Isolated Systolic Hypertension Among Middle-Aged and Elderly US Hypertensives. Hypertension. 2001 Mar 1;37(3):869–74.

8. Smulyan H, Mookherjee S, Safar ME. The two faces of hypertension: role of aortic stiffness. J Am Soc Hypertens. 2016 Feb;10(2):175–83.

9. Townsend RR, Wilkinson IB, Schiffrin EL, Avolio AP, Chirinos JA, Cockcroft JR, et al. Recommendations for Improving and Standardizing Vascular Research on Arterial Stiffness. Hypertension. 2015 Sep;66(3):698–722.

10. Wagenseil JE, Mecham RP. Vascular Extracellular Matrix and Arterial Mechanics. Physiol Rev. 2009 Jul 1;89(3):957–89.

11. Briones AM, Arribas SM, Salaices M. Role of extracellular matrix in vascular remodeling of hypertension: Curr Opin Nephrol Hypertens. 2010 Mar;19(2):187–94.

12. Tsamis A, Krawiec JT, Vorp DA. Elastin and collagen fibre microstructure of the human aorta in ageing and disease: a review. J R Soc Interface [Internet]. 2013 Jun 6 [cited 2016 Apr 24];10(83). Available from: http://www.ncbi.nlm.nih.gov/pmc/articles/PMC3645409/

13. Oudegeest-Sander MH, Rikkert MGMO, Smits P, Thijssen DHJ, van Dijk APJ, Levine BD, et al. The effect of an advanced glycation end-product crosslink breaker and exercise training on vascular function in older individuals: a randomized factorial design trial. Exp Gerontol. 2013 Dec;48(12):1509–17.

14. Sehgel NL, Sun Z, Hong Z, Hunter WC, Hill MA, Vatner DE, et al. Augmented Vascular Smooth Muscle Cell Stiffness and Adhesion When Hypertension Is Superimposed on Aging. Hypertension. 2015 Feb 1;65(2):370–7.

15. Intengan HD, Thibault G, Li J-S, Schiffrin EL. Resistance Artery Mechanics, Structure, and Extracellular Components in Spontaneously Hypertensive Rats Effects of Angiotensin Receptor Antagonism and Converting Enzyme Inhibition. Circulation. 1999 Nov 30;100(22):2267–75.

16. Briet M, Boutouyrie P, Laurent S, London GM. Arterial stiffness and pulse pressure in CKD and ESRD. Kidney Int. 2012 Aug;82(4):388–400.

17. O'Rourke MF, Hashimoto J. Mechanical Factors in Arterial Aging: A Clinical Perspective. J Am Coll Cardiol. 2007 Jul 3;50(1):1–13.

18. Maron BJ. Hypertrophic Cardiomyopathy: A Systematic Review. JAMA. 2002 Mar 13;287(10):1308–20.

19. Tritakis V, Tzortzis S, Ikonomidis I, Dima K, Pavlidis G, Trivilou P, et al. Association of arterial stiffness with coronary flow reserve in revascularized coronary artery disease patients. World J Cardiol. 2016 Feb 26;8(2):231–9.

20. Mattace-Raso FUS, Cammen TJM van der, Hofman A, Popele NM van, Bos ML, Schalekamp MADH, et al. Arterial Stiffness and Risk of Coronary Heart Disease and Stroke. Circulation. 2006 Feb 7;113(5):657–63.

21. Watanabe H, Ohtsuka S, Kakihana M, Sugishita Y. Coronary circulation in dogs with an experimental decrease in aortic compliance. J Am Coll Cardiol. 1993 May 1;21(6):1497–506.

22. Vlachopoulos C, Aznaouridis K, Stefanadis C. Prediction of Cardiovascular Events and All-Cause Mortality With Arterial Stiffness: A Systematic Review and Meta-Analysis. J Am Coll Cardiol. 2010 Mar 30;55(13):1318–27.

23. Pase MP, Beiser A, Himali JJ, Tsao C, Satizabal CL, Vasan RS, et al. Aortic Stiffness and the Risk of Incident Mild Cognitive Impairment and Dementia. Stroke. 2016 Sep 1;47(9):2256–61.

24. Hanon O, Haulon S, Lenoir H, Seux M-L, Rigaud A-S, Safar M, et al. Relationship Between Arterial Stiffness and Cognitive Function in Elderly Subjects With Complaints of Memory Loss. Stroke. 2005 Oct 1;36(10):2193–7.

25. Sedaghat S, Mattace-Raso FUS, Hoorn EJ, Uitterlinden AG, Hofman A, Ikram MA, et al. Arterial Stiffness and Decline in Kidney Function. Clin J Am Soc Nephrol. 2015 Dec 7;10(12):2190–7.

26. Madero M, Peralta C, Katz R, Canada R, Fried L, Najjar S, et al. Association of Arterial Rigidity with Incident Kidney Disease and Kidney Function Decline: The Health ABC Study. Clin J Am Soc Nephrol. 2013 Mar 7;8(3):424–33.

27. Garnier A-S, Briet M. Arterial Stiffness and Chronic Kidney Disease. Pulse. 2016 Apr;3(3–4):229–41.

28. Schiffrin EL. Vascular stiffening and arterial compliance Implications for systolic blood pressure. Am J Hypertens. 2004 Dec 1;17(S3):39S–48S.

29. Harvey A, Montezano AC, Lopes RA, Rios F, Touyz RM. Vascular Fibrosis in Aging and Hypertension: Molecular Mechanisms and Clinical Implications. Can J Cardiol. 2016 May;32(5):659–68.

30. Wynn TA, Ramalingam TR. Mechanisms of fibrosis: therapeutic translation for fibrotic disease. Nat Med. 2012 Jul 6;18(7):1028–40.

31. Hinz B, Phan SH, Thannickal VJ, Prunotto M, Desmoulière A, Varga J, et al. Recent Developments in Myofibroblast Biology. Am J Pathol. 2012 Apr;180(4):1340–55.

32. Hinz B. Formation and Function of the Myofibroblast during Tissue Repair. J Invest Dermatol. 2007 Mar;127(3):526–37.

33. Klingberg F, Hinz B, White ES. The myofibroblast matrix: implications for tissue repair and fibrosis. J Pathol. 2013 Jan;229(2):298–309.

34. Baek HA, Kim DS, Park HS, Jang KY, Kang MJ, Lee DG, et al. Involvement of endoplasmic reticulum stress in myofibroblastic differentiation of lung fibroblasts. Am J Respir Cell Mol Biol. 2012 Jun;46(6):731–9.

35. Zhong Q, Zhou B, Ann DK, Minoo P, Liu Y, Banfalvi A, et al. Role of Endoplasmic Reticulum Stress in Epithelial-Mesenchymal Transition of Alveolar Epithelial Cells. Am J Respir Cell Mol Biol. 2011 Sep;45(3):498–509.

36. Carlisle RE, Heffernan A, Brimble E, Liu L, Jerome D, Collins CA, et al. TDAG51 mediates epithelial-to-mesenchymal transition in human proximal tubular epithelium. Am J Physiol - Ren Physiol. 2012 Aug 1;303(3):F467–81.

37. Wenzel SE, Balzar S. Myofibroblast or Smooth Muscle. Am J Respir Crit Care Med. 2006 Aug 15;174(4):364–5.

38. Ford CM, Li S, Pickering JG. Angiotensin II Stimulates Collagen Synthesis in Human Vascular Smooth Muscle Cells Involvement of the AT1 Receptor, Transforming Growth Factor-β, and Tyrosine Phosphorylation. Arterioscler Thromb Vasc Biol. 1999 Aug 1;19(8):1843–51.

39. Satoh C, Fukuda N, Hu WY, Nakayama M, Kishioka H, Kanmatsuse K. Role of endogenous angiotensin II in the increased expression of growth factors in vascular smooth muscle cells from spontaneously hypertensive rats. J Cardiovasc Pharmacol. 2001 Jan;37(1):108–18.

40. Schlumberger W, Thie M, Rauterberg J, Robenek H. Collagen synthesis in cultured aortic smooth muscle cells. Modulation by collagen lattice culture, transforming growth factor-beta 1, and epidermal growth factor. Arterioscler Thromb Vasc Biol. 1991 Nov 1;11(6):1660–6.

41. Kubota K, Okazaki J, Louie O, Kent KC, Liu B. TGF-β stimulates collagen (I) in vascular smooth muscle cells via a short element in the proximal collagen promoter. J Surg Res. 2003 Jan;109(1):43–50.

42. Lu P, Wang S, Cai W, Sheng J. Role of TGF-β1/Smad3 Signaling Pathway in Secretion of Type I and III Collagen by Vascular Smooth Muscle Cells of Rats Undergoing Balloon Injury. J Biomed Biotechnol [Internet]. 2012 [cited 2015 Feb 3];2012. Available from: http://www.ncbi.nlm.nih.gov/pmc/articles/PMC3471068/

43. Weigert C, Brodbeck K, Klopfer K, Häring H, Schleicher E. Angiotensin II induces human TGF-β1 promoter activation: similarity to hyperglycaemia. Diabetologia. 2002 Jun 1;45(6):890–8.

44. Nataatmadja M, West J, Prabowo S, West M. Angiotensin II Receptor Antagonism Reduces Transforming Growth Factor Beta and Smad Signaling in Thoracic Aortic Aneurysm. Ochsner J. 2013;13(1):42–8.

45. Sorescu D. Smad3 Mediates Angiotensin II– and TGF-β1–Induced Vascular Fibrosis Smad3 Thickens the Plot. Circ Res. 2006 Apr 28;98(8):988–9.

46. Yang F, Chung ACK, Huang XR, Lan HY. Angiotensin II Induces Connective Tissue Growth Factor and Collagen I Expression via Transforming Growth Factor–

β–Dependent and –Independent Smad Pathways The Role of Smad3. Hypertension. 2009 Oct 1;54(4):877–84.

47. Giannandrea M, Parks WC. Diverse functions of matrix metalloproteinases during fibrosis. Dis Model Mech. 2014 Feb 1;7(2):193–203.

48. Wang M, Zhao D, Spinetti G, Zhang J, Jiang L-Q, Pintus G, et al. Matrix Metalloproteinase 2 Activation of Transforming Growth Factor-β1 (TGF-β1) and TGF-β1–Type II Receptor Signaling Within the Aged Arterial Wall. Arterioscler Thromb Vasc Biol. 2006 Jul 1;26(7):1503–9.

49. McKleroy W, Lee T-H, Atabai K. Always cleave up your mess: targeting collagen degradation to treat tissue fibrosis. Am J Physiol - Lung Cell Mol Physiol. 2013 Jun 1;304(11):L709–21.

50. Ferreira LR, Norris K, Smith T, Hebert C, Sauk JJ. Association of Hsp47, Grp78, and Grp94 with procollagen supports the successive or coupled action of molecular chaperones. J Cell Biochem. 1994 Dec;56(4):518–26.

51. Wilson R, Lees JF, Bulleid NJ. Protein disulfide Isomerase Acts as a Molecular Chaperone during the Assembly of Procollagen. J Biol Chem. 1998 Apr 17;273(16):9637–43.

52. Davidson JM, LuValle PA, Zoia O, Quaglino D, Giro M. Ascorbate Differentially Regulates Elastin and Collagen Biosynthesis in Vascular Smooth Muscle Cells and Skin Fibroblasts by Pretranslational Mechanisms. J Biol Chem. 1997 Jan 3;272(1):345–52.

53. Lawson WE, Cheng D-S, Degryse AL, Tanjore H, Polosukhin VV, Xu XC, et al. Endoplasmic reticulum stress enhances fibrotic remodeling in the lungs. Proc Natl Acad Sci U S A. 2011 Jun 28;108(26):10562–7.

54. Tanjore H, Blackwell TS, Lawson WE. Emerging evidence for endoplasmic reticulum stress in the pathogenesis of idiopathic pulmonary fibrosis. Am J Physiol Lung Cell Mol Physiol. 2012 Apr 15;302(8):L721-729.

55. Ayaub EA, Kolb PS, Mohammed-Ali Z, Tat V, Murphy J, Bellaye P-S, et al. GRP78 and CHOP modulate macrophage apoptosis and the development of bleomycin-induced pulmonary fibrosis. J Pathol. 2016 Aug;239(4):411–25.

56. Kassan M, Galán M, Partyka M, Saifudeen Z, Henrion D, Trebak M, et al. Endoplasmic Reticulum Stress Is Involved in Cardiac Damage and Vascular Endothelial Dysfunction in Hypertensive Mice. Arterioscler Thromb Vasc Biol. 2012 Jul 1;32(7):1652–61.

57. Chiang C-K, Hsu S-P, Wu C-T, Huang J-W, Cheng H-T, Chang Y-W, et al. Endoplasmic Reticulum Stress Implicated in the Development of Renal Fibrosis. Mol Med. 2011;17(11–12):1295–305.

58. Spitler KM, Webb RC. Endoplasmic Reticulum Stress Contributes to Aortic Stiffening via Proapoptotic and Fibrotic Signaling Mechanisms. Hypertension. 2014 Mar 1;63(3):e40–5.

59. Ron D, Walter P. Signal integration in the endoplasmic reticulum unfolded protein response. Nat Rev Mol Cell Biol. 2007 Jul;8(7):519–29.

60. Hetz C. The unfolded protein response: controlling cell fate decisions under ER stress and beyond. Nat Rev Mol Cell Biol. 2012 Feb;13(2):89–102.

61. Dickhout JG, Krepinsky JC. Endoplasmic Reticulum Stress and Renal Disease. Antioxid Redox Signal. 2009 Jun 9;11(9):2341–52.

62. Chen Y, Brandizzi F. IRE1: ER stress sensor and cell fate executor. Trends Cell Biol [Internet]. 2013 Nov [cited 2016 Nov 28];23(11). Available from: http://www.ncbi.nlm.nih.gov/pmc/articles/PMC3818365/

63. Upton J-P, Wang L, Han D, Wang ES, Huskey NE, Lim L, et al. IRE1α Cleaves Select microRNAs During ER Stress to Derepress Translation of Proapoptotic Caspase-2. Science. 2012 Nov 9;338(6108):818–22.

64. Han D, Lerner AG, Walle LV, Upton J-P, Xu W, Hagen A, et al. IRE1α Kinase Activation Modes Control Alternate Endoribonuclease Outputs to Determine Divergent Cell Fates. Cell. 2009 Aug 7;138(3):562–75.

65. Acosta-Alvear D, Zhou Y, Blais A, Tsikitis M, Lents NH, Arias C, et al. XBP1 Controls Diverse Cell Type- and Condition-Specific Transcriptional Regulatory Networks. Mol Cell. 2007 Jul 6;27(1):53–66.

66. Dickhout JG, Lhoták Š, Hilditch BA, Basseri S, Colgan SM, Lynn EG, et al. Induction of the unfolded protein response after monocyte to macrophage differentiation augments cell survival in early atherosclerotic lesions. FASEB J. 2011 Feb 1;25(2):576–89.

67. Iwakoshi NN, Lee A-H, Vallabhajosyula P, Otipoby KL, Rajewsky K, Glimcher LH. Plasma cell differentiation and the unfolded protein response intersect at the transcription factor XBP-1. Nat Immunol. 2003 Apr;4(4):321–9.

68. Iwakoshi NN, Lee A-H, Glimcher LH. The X-box binding protein-1 transcription factor is required for plasma cell differentiation and the unfolded protein response. Immunol Rev. 2003 Aug 1;194(1):29–38.

69. Cross BCS, Bond PJ, Sadowski PG, Jha BK, Zak J, Goodman JM, et al. The molecular basis for selective inhibition of unconventional mRNA splicing by an IRE1-binding small molecule. Proc Natl Acad Sci U S A. 2012 Apr 10;109(15):E869–78.

70. Ali MMU, Bagratuni T, Davenport EL, Nowak PR, Silva-Santisteban MC, Hardcastle A, et al. Structure of the Ire1 autophosphorylation complex and implications for the unfolded protein response. EMBO J. 2011 Mar 2;30(5):894–905.

71. Carlisle RE, Brimble E, Werner KE, Cruz GL, Ask K, Ingram AJ, et al. 4-Phenylbutyrate Inhibits Tunicamycin-Induced Acute Kidney Injury via CHOP/GADD153 Repression. PLoS ONE. 2014 Jan 8;9(1):e84663.

72. Luo T, Kim JK, Chen B, Abdel-Latif A, Kitakaze M, Yan L. Attenuation of ER stress prevents post-infarction-induced cardiac rupture and remodeling by modulating both cardiac apoptosis and fibrosis. Chem Biol Interact. 2015 Jan 5;225:90.

73. Tanaka Y, Ishitsuka Y, Hayasaka M, Yamada Y, Miyata K, Endo M, et al. The exacerbating roles of CCAAT/enhancer-binding protein homologous protein (CHOP) in the development of bleomycin-induced pulmonary fibrosis and the preventive effects of tauroursodeoxycholic acid (TUDCA) against pulmonary fibrosis in mice. Pharmacol Res. 2015 Sep;99:52–62.

74. Yu H, Clarke MCH, Figg N, Littlewood TD, Bennett MR. Smooth Muscle Cell Apoptosis Promotes Vessel Remodeling and Repair via Activation of Cell Migration, Proliferation, and Collagen Synthesis. Arterioscler Thromb Vasc Biol. 2011 Nov 1;31(11):2402–9.

75. Liu S-H, Yang C-C, Chan D-C, Wu C-T, Chen L-P, Huang J-W, et al. Chemical chaperon 4-phenylbutyrate protects against the endoplasmic reticulum stress-mediated renal fibrosis in vivo and in vitro. Oncotarget. 2016 Mar 3;7(16):22116–27.

76. Choi S-K, Lim M, Byeon S-H, Lee Y-H. Inhibition of endoplasmic reticulum stress improves coronary artery function in the spontaneously hypertensive rats. Sci Rep [Internet]. 2016 Aug 23 [cited 2016 Nov 11];6. Available from: http://www.ncbi.nlm.nih.gov/pmc/articles/PMC4994042/

77. Olivares S, Henkel AS. Hepatic Xbp1 Gene Deletion Promotes Endoplasmic Reticulum Stress-induced Liver Injury and Apoptosis. J Biol Chem. 2015 Dec 11;290(50):30142–51.

78. Fu HY, Okada K, Liao Y, Tsukamoto O, Isomura T, Asai M, et al. Ablation of C/EBP Homologous Protein Attenuates Endoplasmic Reticulum–Mediated Apoptosis and Cardiac Dysfunction Induced by Pressure Overload. Circulation. 2010 Jul 27;122(4):361–9.

79. Chen L, Zhao M, Li J, Wang Y, Bao Q, Wu S, et al. Critical role of X-box binding protein 1 in NADPH oxidase 4-triggered cardiac hypertrophy is mediated by receptor interacting protein kinase 1. Cell Cycle. 2016 Dec 8;0(ja):00–00.

80. Duan Q, Chen C, Yang L, Li N, Gong W, Li S, et al. MicroRNA regulation of unfolded protein response transcription factor XBP1 in the progression of cardiac hypertrophy and heart failure in vivo. J Transl Med [Internet]. 2015 Nov 16 [cited 2016 Nov 11];13. Available from: http://www.ncbi.nlm.nih.gov/pmc/articles/PMC4647486/

81. Duan Q, Ni L, Wang P, Chen C, Yang L, Ma B, et al. Deregulation of XBP1 expression contributes to myocardial vascular endothelial growth factor-A expression and angiogenesis during cardiac hypertrophy in vivo. Aging Cell. 2016 Aug;15(4):625.

82. Wu J, Saleh MA, Kirabo A, Itani HA, Montaniel KRC, Xiao L, et al. Immune activation caused by vascular oxidation promotes fibrosis and hypertension. J Clin Invest. 2015 Nov 23;126(1):50–67.

83. Moore JP, Vinh A, Tuck KL, Sakkal S, Krishnan SM, Chan CT, et al. M2 macrophage accumulation in the aortic wall during angiotensin II infusion in mice is associated with fibrosis, elastin loss, and elevated blood pressure. Am J Physiol - Heart Circ Physiol. 2015 Sep 1;309(5):H906–17.

84. Mohammed-Ali Z, Cruz GL, Dickhout JG. Crosstalk between the Unfolded Protein Response and NF-κB-Mediated Inflammation in the Progression of Chronic Kidney Disease. J Immunol Res [Internet]. 2015 [cited 2016 Dec 9];2015. Available from: https://www-ncbi-nlm-nih-gov.libaccess.lib.mcmaster.ca/pmc/articles/PMC4419235/

85. Matsuzaki S, Hiratsuka T, Taniguchi M, Shingaki K, Kubo T, Kiya K, et al. Physiological ER Stress Mediates the Differentiation of Fibroblasts. PLoS ONE [Internet]. 2015 Apr 30 [cited 2015 Jun 16];10(4). Available from: http://www.ncbi.nlm.nih.gov/pmc/articles/PMC4416017/

86. Tanjore H, Cheng D-S, Degryse AL, Zoz DF, Abdolrasulnia R, Lawson WE, et al. Alveolar Epithelial Cells Undergo Epithelial-to-Mesenchymal Transition in Response to Endoplasmic Reticulum Stress. J Biol Chem. 2011 Sep 2;286(35):30972–80.

87. Mo X-T, Zhou W-C, Cui W-H, Li D-L, Li L-C, Xu L, et al. Inositol-requiring protein 1 – X-box-binding protein 1 pathway promotes epithelial–mesenchymal transition via mediating snail expression in pulmonary fibrosis. Int J Biochem Cell Biol. 2015 Aug;65:230–8.

88. Heindryckx F, Binet F, Ponticos M, Rombouts K, Lau J, Kreuger J, et al. Endoplasmic reticulum stress enhances fibrosis through IRE1α-mediated degradation of miR-150 and XBP-1 splicing. EMBO Mol Med. 2016 Jul;8(7):729–44.

89. Kim RS, Hasegawa D, Goossens N, Tsuchida T, Athwal V, Sun X, et al. The XBP1 Arm of the Unfolded Protein Response Induces Fibrogenic Activity in Hepatic Stellate Cells Through Autophagy. Sci Rep [Internet]. 2016 [cited 2017 Jan 3];6. Available from: https://www-ncbi-nlm-nih-gov.libaccess.lib.mcmaster.ca/pmc/articles/PMC5172197/

90. Lee A-H, Iwakoshi NN, Glimcher LH. XBP-1 Regulates a Subset of Endoplasmic Reticulum Resident Chaperone Genes in the Unfolded Protein Response. Mol Cell Biol. 2003 Nov;23(21):7448–59.

91. Van Duyn Graham L, Sweetwyne MT, Pallero MA, Murphy-Ullrich JE. Intracellular Calreticulin Regulates Multiple Steps in Fibrillar Collagen Expression, Trafficking, and Processing into the Extracellular Matrix. J Biol Chem. 2010 Mar 5;285(10):7067–78.

92. Hall KL, Harding JW, Hosick HL. Isolation and characterization of clonal vascular smooth muscle cell lines from spontaneously hypertensive and normotensive rat aortas. Vitro Cell Dev Biol J Tissue Cult Assoc. 1991 Oct;27A(10):791–8.

93. Carlisle RE, Werner KE, Yum V, Lu C, Tat V, Memon M, et al. Endoplasmic reticulum stress inhibition reduces hypertension through the preservation of resistance blood vessel structure and function. J Hypertens. 2016 Apr 23;

94. Rodríguez JP, Montecinos L, Ríos S, Reyes P, Martínez J. Mesenchymal stem cells from osteoporotic patients produce a type I collagen-deficient extracellular matrix favoring adipogenic differentiation. J Cell Biochem. 2000 Dec 15;79(4):557–65.

95. Xu Q, Norman JT, Shrivastav S, Lucio-Cazana J, Kopp JB. In vitro models of TGF-β-induced fibrosis suitable for high-throughput screening of antifibrotic agents. Am J Physiol - Ren Physiol. 2007 Aug 1;293(2):F631–40.

96. Nicosia RF, Ottinetti A. Growth of microvessels in serum-free matrix culture of rat aorta. A quantitative assay of angiogenesis in vitro. Lab Investig J Tech Methods Pathol. 1990 Jul;63(1):115–22.

97. Lomashvili KA, Cobbs S, Hennigar RA, Hardcastle KI, O'Neill WC. Phosphate-Induced Vascular Calcification: Role of Pyrophosphate and Osteopontin. J Am Soc Nephrol. 2004 Jun 1;15(6):1392–401.

98. Calfon M, Zeng H, Urano F, Till JH, Hubbard SR, Harding HP, et al. IRE1α couples endoplasmic reticulum load to secretory capacity by processing the XBP-1 mRNA. Nature. 2002 Jan 3;415(6867):92–6.

99. Zimmerman KA, Graham LV, Pallero MA, Murphy-Ullrich JE. Calreticulin (CRT) regulates Transforming Growth Factor-β (TGF-β) stimulated extracellular matrix production. J Biol Chem. 2013 Apr 5;jbc.M112.447243.

100. Kawasaki K, Ushioda R, Ito S, Ikeda K, Masago Y, Nagata K. Deletion of the Collagen-specific Molecular Chaperone Hsp47 Causes Endoplasmic Reticulum Stress-mediated Apoptosis of Hepatic Stellate Cells. J Biol Chem. 2014 Dec 18;jbc.M114.592139.

101. Marutani T, Yamamoto A, Nagai N, Kubota H, Nagata K. Accumulation of type IV collagen in dilated ER leads to apoptosis in Hsp47-knockout mouse embryos via induction of CHOP. J Cell Sci. 2004 Nov 15;117(24):5913–22.

102. Rocnik EF, Veer E van der, Cao H, Hegele RA, Pickering JG. Functional Linkage between the Endoplasmic Reticulum Protein Hsp47 and Procollagen Expression in Human Vascular Smooth Muscle Cells. J Biol Chem. 2002 Oct 11;277(41):38571–8.

103. Ferreira LR, Norris K, Smith T, Hebert C, Sauk JJ. Hsp47 and other ER-resident molecular chaperones form heterocomplexes with each other and with collagen type IV chains. Connect Tissue Res. 1996;33(4):265–73.

104. Lee G-H, Oh H-W, Lim H-D, Lee W, Chae H-J, Kim H-R. 4-phenylbutyric Acid Regulates Collagen Synthesis and Secretion Induced by High Concentrations of Glucose in Human Gingival Fibroblasts. Korean J Physiol Pharmacol Off J Korean Physiol Soc Korean Soc Pharmacol. 2011 Dec;15(6):345.

105. Rishikof DC, Ricupero DA, Liu H, Goldstein RH. Phenylbutyrate decreases type I collagen production in human lung fibroblasts. J Cell Biochem. 2004 Mar 1;91(4):740–8.

106. Walter F, Schmid J, Düssmann H, Concannon CG, Prehn JHM. Imaging of single cell responses to ER stress indicates that the relative dynamics of IRE1/XBP1 and PERK/ATF4 signalling rather than a switch between signalling branches determine cell survival. Cell Death Differ. 2015 Sep;22(9):1502–16.

107. Hetz C, Glimcher LH. Fine tuning of the Unfolded Protein Response: Assembling the IRE1α interactome. Mol Cell. 2009 Sep 11;35(5):551–61.

108. Akiyoshi T, Ota H, Iijima K, Son B-K, Kahyo T, Setou M, et al. A novel organ culture model of aorta for vascular calcification. Atherosclerosis. 2016 Jan;244:51–8.

109. Isabelle M, Simonet S, Ragonnet C, Sansilvestri-Morel P, Clavreul N, Vayssettes-Courchay C, et al. Chronic reduction of nitric oxide level in adult spontaneously hypertensive rats induces aortic stiffness similar to old spontaneously hypertensive rats. J Vasc Res. 2012;49(4):309–18.

110. Ono H, Ono Y, Frohlich ED. ACE Inhibition Prevents and Reverses L-NAMEExacerbated Nephrosclerosis in Spontaneously Hypertensive Rats. Hypertension. 1996 Feb 1;27(2):176–83.

111. Ono H, Ono Y, Frohlich ED. Nitric Oxide Synthase Inhibition in Spontaneously Hypertensive Rats Systemic, Renal, and Glomerular Hemodynamics. Hypertension. 1995 Aug 1;26(2):249–55.

112. Zhou X, Ono H, Ono Y, Frohlich ED. Aldosterone Antagonism Ameliorates Proteinuria and Nephrosclerosis Independent of Glomerular Dynamics in L-NAME/SHR Model. Am J Nephrol. 2004 Apr;24(2):242–9.

113. Akashiba A, Ono H, Ono Y, Ishimitsu T, Matsuoka H. Valsartan improves l-NAME-exacerbated cardiac fibrosis with TGF-β inhibition and apoptosis induction in spontaneously hypertensive rats. J Cardiol. 2008 Dec 1;52(3):239–46.

114. Biwer LA, D'souza KM, Abidali A, Tu D, Siniard AL, DeBoth M, et al. Time course of cardiac inflammation during nitric oxide synthase inhibition in SHR: impact of prior transient ACE inhibition. Hypertens Res Off J Jpn Soc Hypertens. 2016 Jan;39(1):8–18.

115. Souza HCD, Ballejo G, Salgado MCO, Silva VJDD, Salgado HC. Cardiac sympathetic overactivity and decreased baroreflex sensitivity in l-NAME hypertensive rats. Am J Physiol - Heart Circ Physiol. 2001 Feb 1;280(2):H844–50.

116. Urabe G, Hoshina K, Shimanuki T, Nishimori Y, Miyata T, Deguchi J. Structural analysis of adventitial collagen to feature aging and aneurysm formation in human aorta. J Vasc Surg. 2016 May;63(5):1341–50.

117. Isabelle M, Chimenti S, Beaussier H, Gransagne D, Villeneuve N, Safar ME, et al. SBP, DBP, and pulse blood pressure variability are temporally associated with the increase in pulse wave velocity in a model of aortic stiffness: J Hypertens. 2016 Apr;34(4):666–75.

118. Bhatta A, Yao L, Toque HA, Shatanawi A, Xu Z, Caldwell RB, et al. Angiotensin II-Induced Arterial Thickening, Fibrosis and Stiffening Involves Elevated Arginase Function. PLoS ONE [Internet]. 2015 Mar 25 [cited 2015 Aug 20];10(3). Available from: http://www.ncbi.nlm.nih.gov/pmc/articles/PMC4373900/

119. Eberson LS, Sanchez PA, Majeed BA, Tawinwung S, Secomb TW, Larson DF. Effect of Lysyl Oxidase Inhibition on Angiotensin II-Induced Arterial Hypertension, Remodeling, and Stiffness. PLoS ONE [Internet]. 2015 Apr 13 [cited 2016 Jan 13];10(4). Available from: http://www.ncbi.nlm.nih.gov/pmc/articles/PMC4395147/

120. Rodríguez JP, Montecinos L, Ríos S, Reyes P, Martínez J. Mesenchymal stem cells from osteoporotic patients produce a type I collagen-deficient extracellular matrix favoring adipogenic differentiation. J Cell Biochem. 2000 Sep 14;79(4):557–65.

121. Group TSR. A Randomized Trial of Intensive versus Standard Blood-Pressure Control. N Engl J Med. 2015 Nov 26;373(22):2103–16.

122. Koumaras C, Tziomalos K, Stavrinou E, Katsiki N, Athyros VG, Mikhailidis DP, et al. Effects of renin-angiotensin-aldosterone system inhibitors and beta-blockers on markers of arterial stiffness. J Am Soc Hypertens. 2014 Feb;8(2):74–82.

123. Koumaras C, Tzimou M, Stavrinou E, Griva T, Gossios TD, Katsiki N, et al. Role of Antihypertensive Drugs in Arterial "De-Stiffening" and Central Pulsatile Hemodynamics. Am J Cardiovasc Drugs. 2012 Jun 1;12(3):143–56.

124. Hetz C, Chevet E, Harding HP. Targeting the unfolded protein response in disease. Nat Rev Drug Discov. 2013 Sep;12(9):703–19.

125. Xu T, Yang L, Yan C, Wang X, Huang P, Zhao F, et al. The IRE1α-XBP1 pathway regulates metabolic stress-induced compensatory proliferation of pancreatic β-cells. Cell Res. 2014 Sep;24(9):1137–40.